Luis Felipe Del Carpio Vega

System level modeling and evaluation of advanced linear interference aware receivers

School of Electrical Engineering

Thesis submitted for examination for the degree of Master of Science in Technology.

Espoo 13.08.2012

Thesis supervisor:

Prof. Olav Tirkkonen

Thesis instructor:

D.Sc. (Tech.) Mihai Enescu

Aalto University
School of Electrical Engineering

AALTO UNIVERSITY
SCHOOL OF ELECTRICAL ENGINEERING

ABSTRACT OF THE
MASTER'S THESIS

Author: Luis Felipe Del Carpio Vega

Title: System level modeling and evaluation of advanced linear interference aware receivers

Date: 13.08.2012 Language: English Number of pages:8+63

Department of Communications and Networking

Professorship: Radio Communications Code: S-72

Supervisor: Prof. Olav Tirkkonen

Instructor: D.Sc. (Tech.) Mihai Enescu

To cope with the growth of data traffic through mobile networks, efficient utilization of the available radio spectrum is needed. In densely deployed radio networks, User Equipments (UE) will experience high levels of interference which limits the achievable spectral efficiency. In this case, a way to improve the achievable performance is by mitigating interference at the UE side.
Advanced linear interference aware receivers are linear receivers able to mitigate external co-channel interference. Optimum linear interference rejection is obtained with the Interference Rejection Combining (IRC) receiver which relies on the ideal knowledge of the interference covariance matrix. The IRC interference covariance matrix is the sum of all interference channel covariance matrices. In practical radio networks, like LTE-Advanced, the knowledge of interference channel covariance matrices might not always be available. However, the IRC interference covariance matrix estimation can be done with a data-based or reference-symbol-based interference covariance matrix estimation algorithm.
In this thesis, the modeling and evaluation of advanced linear interference aware receivers for LTE-Advanced downlink are studied. In particular, the data-based and reference-symbol-based covariance matrix estimation algorithms are modeled by using the Wishart distribution. This modeling allows the evaluation of advanced linear receivers without explicit need for baseband signals. The evaluation is done with a system level simulator. Later, a comparison of performance between advanced linear interference aware receivers and 3GPP baseline linear receivers for multiple homogeneous and heterogeneous deployment scenarios is presented.
Finally, it is shown that advanced linear interference aware receivers can provide spectral efficiency improvements specially to UEs located at cell borders.

Keywords: Interference rejection combining, linear interference aware receiver, covariance matrix estimation, Wishart distribution, modeling, random matrix theory, LTE-Advanced downlink, MIMO

Acknowledgments

This thesis was written in and funded by the Systems Research and Standardization unit of Renesas Mobile Europe, Helsinki, Finland.

First, I would like to thank my instructor D.Sc. Mihai Enescu for considering me eligible for the challenging task and for providing guidance and support during the research period.

Next, I would like to thank my supervisor Professor Olav Tirkkonen for all the advice, time and ideas he gave me, not only during the research period but also during my Master's degree studies.

I would also like to thank all the team working in the Systems Research and Standardization unit at Renesas Mobile Europe, especially M.Sc. Kari Pietikäinen, M.Sc. Markku Kuusela, M.Sc. Marko Lampinen, D.Sc. Timo Roman, D.Sc. Helka-Liina Määttänen. I would like to express my deepest gratitude for teaching me about the LTE system, the simulator's source code, MIMO antenna technology and helping me in refining the concepts and results during the research period.

I would like to thank all my family for being an endless source of support and encouragement. I would like to thank my mother María Victoria and grandfather Enrique for teaching me the values of love and perseverance. I would like to thank my wife Eija for showing extraordinary patience and being always loving. I would like to thank my in-laws Veikko and Kaarina for showing me what Finland means to them.

Helsinki, August 2012

Luis Felipe Del Carpio Vega

Contents

Symbols and abbreviations

Abbreviations

3GPP	Third Generation Partnership Project
CSI	Channel State Information
CRS	Cell-specific Reference Symbols
DMRS	UE-specific Demodulation Reference Symbols
eNB	E-UTRAN Node B
	evolved Node B
HetNet	Heterogeneous Network
HSPA	High-Speed Packet Access
ISD	Inter-Site Distance
ISI	Inter-Symbol Interference
ITU	International Telecommunication Union
IRC	Interference Rejection Combining
LMMSE	Linear Minimum Mean Square Error
$\mathrm{LMMSE-IRC_{WI-DATA}}$	Wishart distribution emulated data-based IRC
$\mathrm{LMMSE-IRC_{RS-DATA}}$	Wishart distribution emulated reference-symbol-based IRC
LTE	Long Term Evolution
LTE-Advanced	Long Term Evolution Advanced
MeNB	Macro eNB
MIMO	Multiple Input Multiple Output
MMSE	Minimum Mean Square Error
MRC	Maximum Ratio Combining
OFDM	Orthogonal Frequency Division Multiplex
	Orthogonal Frequency Division Multiplexing
OFDMA	Orthogonal Frequency Division Multiple Access
PDCCH	Physical Downlink Control Channel
PDSCH	Physical Downlink Shared Channel
PeNB	Pico eNB
PRB	Physical Resource Block
RE	Resource Element
RS	Reference Symbol
RRM	Radio Resource Management
SC-FDMA	Single-Carrier Frequency Division Multiple Access
SE	Spectral Efficiency
SINR	Signal-to-Interference-plus-Noise Ratio
UMa	Urban Macrocell
UMi	Urban Microcell
UE	User Equipment
WCDMA	Wideband Code Division Multiple Access

List of Figures

List of Tables

1 Introduction

Mobile-connected laptops, tablet computers and smartphones are changing the way people use telecommunication services. High-speed mobile data connections, multimedia applications and portable devices which increasingly resemble computers are reasons why mobile data traffic is continuously increasing through mobile networks. According to the latest traffic reports [1, 2], mobile data traffic has doubled from the second quarter of 2010 to the second quarter of 2011 and a 26-fold increase is predicted by 2015 compared with 2010.

In order to cope with the ever-increasing mobile data traffic demand, continuous enhancements to deployed mobile radio access systems and mobile network architectures have been made, for example the WCDMA radio access system evolved to HSPA+ with an enhanced radio interface and a flat network architecture. Also, small-cells (pico-cells / femto-cells) have been deployed as complementary to macro-cells to increase the achievable data rates and coverage when needed.

The Third Generation Partnership Project (3GPP) continued the development of radio access networks by introducing the Long-Term Evolution (LTE) radio system as Release 8, later LTE enhancements were standardized as Release 9. In Release 10, LTE evolved to become LTE-Advanced which is designed to meet all ITU-R requirements for an IMT-Advanced radio technology [3].

During Release 11, User Equipment (UE) advanced linear interference aware receivers, or interference suppression receivers, are investigated in order to assess the performance improvement they bring to LTE cell-edge users. Other investigated interference cancellation techniques are based on network coordination, for example Coordinated Multi-point Transmission (CoMP) and Enhanced Inter-cell Interference Coordination (eICIC).

In this thesis, the focus is on modeling and evaluation of advanced linear interference aware receivers in the context of LTE-Advanced downlink. There is a belief that in many LTE-Advanced deployment scenarios there exists a dominant source of interference that can be mitigated by using the Interference Rejection Combining receiver (IRC), also called the optimum linear combiner. The existence of a dominant source of interference is indeed analyzed and shown in Chapter 5 by using an LTE-Advanced system level simulator.

The IRC receiver utilizes an ideal interference covariance matrix to perform the optimum linear rejection. Ideally the interference covariance matrix is the sum of all interference channel covariance matrices which implies the ideal knowledge of interference channels. In practical radio networks, like LTE-Advanced, the knowledge of interference channels for interference covariance matrix calculation might not always be available. However, practical IRC algorithms estimate the interference covariance matrix, for example by utilizing received data signals or pilot signals. This make possible the study of IRC algorithms for example in link level simulators where baseband signal modeling is available. However, without a proper interference environment emulation, the performance assessment of practical IRC algorithms is challenging.

System level simulators are designed to model more realistic interference environments than link level simulators by including multiple cells, multiple UEs and special channel models like the Spatial Channel Model (SCM) or ITU-R channel models. In system level simulators a large radio network can be studied. On the other hand, system level simulators lack baseband signal modeling, which makes the study of advanced receiver algorithms very challenging.

In this thesis an emulation technique based on random matrix theory for the estimation of the IRC interference covariance matrix has been studied in order to enable the assessment of advanced linear interference aware receiver algorithms without the explicit need for baseband signals. The emulation method was later applied in an LTE system level simulator.

1.1 Background

LTE-Advanced downlink uses an Orthogonal Frequency Division Multiplex (OFDM) radio interface and advanced Multiple Input Multiple Output (MIMO) techniques combined with time/frequency/space Radio Resource Management (RRM) algorithms designed to improve the system capacity. Improvements on the radio-link alone, however are not enough to cope with the increasing traffic demand.

In order to increase system capacity, small-cells and relay nodes deployed under macro-cell coverage complement traditional macro cell deployments and achieve an increase in system capacity by off-loading macro-eNB traffic. This mixed deployment of macro and small cells is called a Heterogeneous Network (HetNet) deployment.

The reduction of Inter-Site Distances (ISD) between macro cell sites results in dense macro cell deployments. Moreover, deployed small-cells share the same frequency resources with macro cells if frequency reuse is one. The combined effect of dense macro cell deployments and small-cells will increase interference levels reducing the Signal-to-Interference-plus-Noise-Ratio (SINR) experienced by User Equipments (UE). In this case, the potential gains of small-cell deployments are limited by interference.

3GPP is currently investigating techniques aimed at reducing interference levels, driven by the need to increase cell-edge capacity. These techniques use either semi-static time domain techniques (e.g. eICIC, FeICIC) or more dynamic techniques such as CoMP. These techniques require different degrees of synchronization and information sharing between radio network elements and could be called transmission-side network-aided interference reduction techniques.

Interference reduction for LTE-Advanced can also be achieved without network aid by means of interference rejection at the UE side. In this thesis, receivers able to reject external co-channel interference are called advanced interference aware receivers. If an UE receiver is aware of the interference structure, it is possible to mitigate it. This increases the post-processing SINR. For example, the Interference Rejection Combining (IRC), or optimum linear combiner [4, 5], is a linear receiver that optimally mitigates both multi-path fading and co-channel interference, achieving spectral efficiency improvements if the spatial information from the interfering signals is completely known by the UE. In contrast, the Maximum Ratio Combining (MRC) receiver is the best choice where Additive White Gaussian Noise (AWGN) is present [6].

The IRC receiver has been studied in the academic literature [4, 5, 6, 7] and proposed for GSM and WCDMA systems. In GSM, the IRC receiver has been investigated in order to improve uplink capacity at base stations [8, 9, 10, 11, 12] whereas Single Antenna Interference Cancellation (SAIC) receivers were studied at the mobile terminal [13, 14, 15, 16]. In WCDMA, the IRC has been studied at both base station [17] and UE side [18, 19, 20].

Previous work on IRC receivers assumed complete knowledge of the IRC interference covariance matrix (e.g. [4, 6, 8]), or have used baseband signals or pilot signals to estimate the IRC interference covariance matrix (e.g. [21, 22]).

In this thesis, the IRC interference covariance matrix estimation procedure is emulated with techniques based on random matrix theory. This allows the study of different algorithms for IRC interference covariance matrix estimation without the need for baseband signals or pilot signals as shown in Chapter 3. Part of this thesis has been also published in [23, 24].

1.2 Motivation

The present thesis focuses on modeling and evaluation of advanced linear interference aware receivers in the context of LTE-Advanced downlink mobile radio system. The focus is on linear receivers because it has been shown that gains expected from non-linear receivers are hard to achieve in presence of channel estimation imperfections [25]. Non-linear receivers also add extra UE signaling and processing complexity.

The motivation for this study arises from the need to obtain an accurate LTE-Advanced system performance after considering different degrees of interference suppression capabilities at the UE side. Generally speaking, an accurate performance analysis of a radio communication system in terms of channel modeling, network topology, radio resource management and complete transmission chain is computationally prohibitive; thus, in order to reduce computational complexity, it is common to perform the analysis from either a system level or a link level perspective. A system level simulator models a multi-cell environment where several UEs are located in different geographical locations but the transmission chain of point-to-point transmissions are not modeled in detail. In contrast, a link level simulator usually models in detail the complete transmission chain for a downlink or uplink point-to-point transmission.

Traditionally, in order to assess the exact performance of linear receiver algorithms, link level analysis is performed by using actual baseband signals. However, link level analysis tends to overlook the complex interference structure experienced by UEs located in different geographical positions in a multi-cell environment. On the other hand, system level analysis takes into account complex interference structures but the study of linear receiver algorithms is challenging due to the lack of baseband signals.

1.3 Objective of the Thesis

The objective of this thesis is the emulation of the IRC interference covariance matrix estimation based on random matrix theory. This emulation allows the modeling of advanced linear interference aware receivers without the need for baseband signals, and thus makes possible the system level evaluation of advanced linear interference aware receivers.

The scope of the thesis is restricted to the LTE-Advanced downlink FDD radio system because of two reasons. First, it is well-known that in mobile data networks there is an asymmetry between downlink and uplink traffic. Downlink has greater traffic demand [26, 27]. Second, enhancements in linear receiver algorithms can increase downlink throughput of cell-edge UEs with small impact on overall system complexity.

1.4 Structure of the Thesis

The thesis is organized as follows. Chaper 2 provides an introduction to LTE-Advanced and MIMO antenna technology. It also gives the signal model used for LTE-Advanced single user MIMO transmission. Chapter 3 introduces the 3GPP baseline linear receivers and advanced linear interference aware receivers with their correspondent modeling. Chapter 4 presents the simulation model used. Chapter 5 discusses what are the interference conditions experienced by UEs in different scenarios and analyzes if dominant interference indeed exists. Chapter 6 summarizes the selected simulation scenarios and assumptions. It also presents and analyzes the simulation results. Finally, Chapter 7 summarizes the most important conclusions and observations and presents some possible future research topics.

2 LTE & LTE-Advanced

LTE and LTE-Advanced are novel radio interfaces specified by 3GPP and designed to become stand-alone systems with packet-switched networking. The LTE radio interface differs from the WCDMA/HSPA radio interface which is based on code-division multiple access. LTE uses an OFDM radio interface for the downlink and Single-Carrier Frequency Division Multiple Access (SC-FDMA) for the uplink [28].

LTE meets the ITU-R IMT requirements for a 3G radio technology, and partially meets the ITU-R IMT-Advanced requirements for a 4G radio technology. The initial LTE specifications were presented in 3GPP Release 8 in 2007 [29], and have evolved in later Releases 9 and 10. The evolution of LTE continued as LTE-Advanced in Release 10 [30]. LTE-Advanced was designed to meet the ITU-R IMT-Advanced requirements [31]. In October 2010, after the ITU assessment process, LTE-Advanced was designated officially as an IMT-Advanced (or 4G) technology [3]. Further improvements to LTE-Advanced will be specified on forthcoming 3GPP Releases 11, 12 and beyond.

In the first part of this chapter, a short technical overview of LTE-Advanced is provided. In addition, the specific differences between LTE and LTE-Advanced will be indicated. LTE-Advanced was designed to have backward compatibility with existing LTE specifications, and thus many design principles and physical layer procedures of LTE are applied in LTE-Advanced.

2.1 An overview of LTE-Advanced

The LTE technical requirements were agreed in June 2005 [32]. The targets for LTE included reduced latency, higher user data rates, improved overall system capacity, and reduced cost of operation compared with its precursors. LTE was required to become a stand-alone system with packet-switched networking. The evolution of the LTE system, its architecture, protocols and performance are described widely in the literature for example [33, 34, 35, 36].

In order to achieve the LTE design targets a flat network architecture based on distributed servers was designed. LTE eNBs having transmission port connections to the core network without intermediate radio network controller nodes were standardized. This was combined with an efficient physical layer. As this thesis focuses on advanced linear interferer aware receivers which are mainly related to the physical layer, details regarding the network architecture will be not be covered. However a good review can be found in [28, 37].

The LTE-Advanced downlink physical layer based on OFDMA and MIMO antenna technology provides new RRM opportunities compared with WCDMA/HSPA and it is mainly optimized for slow moving users. The main design principle is the elimination of Inter-symbol Interference (ISI) and in-cell interference that limit the capacity of WCDMA and HSPA systems [28]. For LTE-Advanced downlink, OFDMA is chosen as the modulation technique because it allows elimination of ISI by using a Cyclic Prefix (CP) with longer duration than the delay spread of the channel. It also allows to use time/frequency RRM techniques allowing better adaptation to changes in channel conditions in both time and frequency domains.

The LTE uplink radio interface employs a Discrete Fourier Transform (DFT)-spread ODFM also called SC-FDMA. Compared with the downlink OFDM, this variation improves the peak-to-average power ratio. This enables more power efficient terminals. As our discussion focuses on the LTE downlink system, further details regarding LTE uplink will be omitted unless they are considered necessary. Further reading about LTE uplink is widely available, e.g. [34].

2.1.1 Physical resource block and resource elements

The minimum LTE-Advanced downlink radio resource addressable for transmission on the time-frequency grid is called Physical Resource Block (PRB) and a single element of the PRB time-frequency grid is called a Resource Elements (RE). A PRB is composed in frequency domain by 12 OFDM sub-carriers spanning 180 kHz (each sub-carrier having a bandwidth of 15 kHz), and it has one millisecond duration in time domain. The PRB time duration is the minimum sub-frame time granularity the LTE-Advanced RRM can handle. Figure 1 depicts a typical PRB.

2.1.2 Downlink physical channels and physical signals

A physical channel corresponds to a set of resource elements carrying information over-the-air. LTE-Advanced defines downlink and uplink physical channels in [38]. A short description of physical channels is given below. A more detailed description of downlink physical channels can be found in [34, 38].

- Physical Broadcast Channel (PBCH), it carries the information needed to access the system.
- Physical Downlink Shared Channel (PDSCH), it carries the user data for point-to-point connections in the downlink direction. All the carried information is intended only for one user.
- Physical Multicast Channel (PMCH), it is intended for carrying multicast/broadcast service content in the downlink direction.
- Physical Control Format Indicator Channel (PCFICH), the PCFICH is use to dynamically indicate how many OFDMA symbols are reserved for control information. This can vary between 1 and 3 for each 1ms sub-frame.
- Physical Downlink Control Channel (PDCCH). An UE will obtain resource allocation information for both downlink and uplink from the PDCCH.
- Physical Hybrid ARQ Indicator Channel (PHICH). The task of the PHICH is simply to indicate in the downlink direction whether an uplink packet was correctly received or not.

A downlink physical signal corresponds to a set of resource elements used by the physical layer but does not carry information originating from higher layers [38]. The following downlink physical signals are defined in LTE-Advanced:

- Reference signal: Reference signals, usually known as pilots, are known symbols transmitted in specific locations within a PRB. They allow UEs to make channel measurements. The derived information from channel measurements can be fed back as CSI or used in the demodulation process. The LTE and LTE-Advanced use different types of reference signals as will be explained later in Section 2.1.4.

- Synchronization signal: There are two kinds of synchronization signals the Primary Synchronization Signal (PSS) and the Secondary Synchronization Signal (SSS). These signals are transmitted, similar to PBCH, always with a bandwidth of 1.08 MHz. They are used for cell identification [34].

2.1.3 Sub-frame structure

An LTE-Advanced FDD frame is composed of 10 sub-frames and a sub-frame is composed by two time slots, each time slot is composed by 6 OFDM symbols with a long CP or 7 OFDM symbols with a short CP depending on the sub-frame configuration.

An LTE-Advanced downlink sub-frame can be configured as:

- Unicast sub-frame: This is an ordinary LTE-Advanced sub-frame where a time slot is composed by 7 OFDM symbols plus a short CP. In this kind of sub-frame the PDCCH can be mapped from 1 up to 3 OFDM symbols starting at the beginning of the first sub-frame time slot, the remaining OFDM symbols are used for PDSCH mapping. Figure 1 depicts this type of configuration.

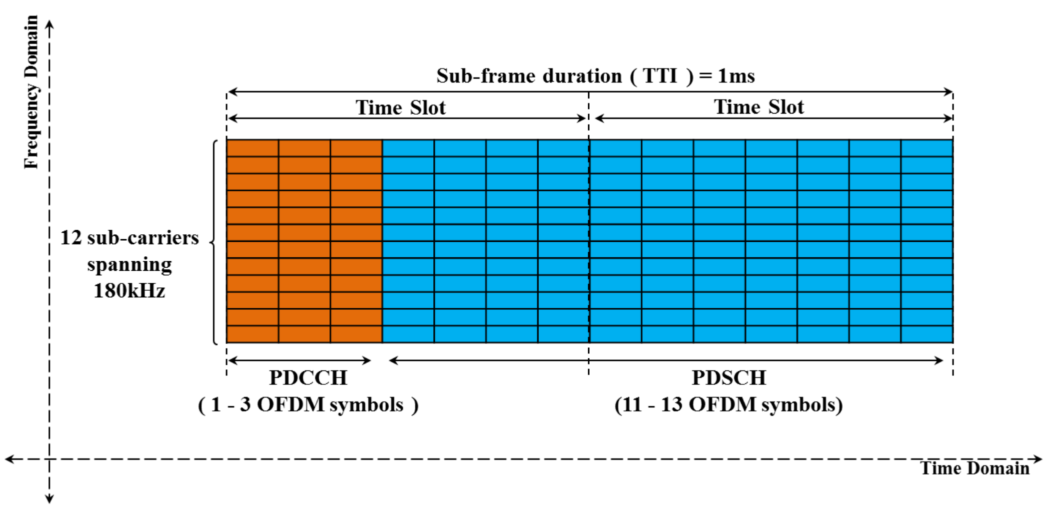

Figure 1: Time-frequency physical resource block

- Multicast sub-frame or MBSFN sub-frame: MBSFN stands for MBMS (Multicast/Broadcast Multimedia Service) over a Single Frequency Network. The

MBSFN was envisaged for delivering services such as Mobile TV. The multicast/broadcast transmission is done using the Multicast Channel (MCH) transport channel mapped on MBSFN sub-frames [33]. The MBSFN transmissions are done over a single frequency network, which means that a set of eNBs transmit the same symbols in a time-synchronized manner, using the same frequency and time resources. All symbols of a MBSFN sub-frame from different cells are received within the same CP. The copies coming from various eNBs are seen by the UE as multiple delayed multi-path components (CP avoids ISI). This enables over-the-air combining which improves the SINR compared with non-MBSFN operation [39].

The MBSFN sub-frame structure standardized in LTE-Advanced is different from a unicast sub-frame. First, the symbols of a multicast sub-frame use a long cyclic prefix, meaning that we have six symbols per time slot or 12 symbols per multicast sub-frame. Second, the multicast sub-frames have less control information overhead (only 1 or 2 symbols) than unicast sub-frames.

2.1.4 Downlink reference signals

The LTE Release 8 and LTE-Advanced Release 10 use different types of reference signals for CSI measurements and channel estimation for demodulation. LTE utilizes Cell-specific Reference Signals (CRS) for both CSI measurements and channel estimation for demodulation. LTE-Advanced utilizes a specific set of RS for CSI measurements called Channel State Information Reference Signals (CSI-RS) and UE-specific demodulation reference signals (DMRS) for channel estimation for demodulation [40]. The characteristics of LTE and LTE-advanced downlink reference signals are explained below [38].

Cell specific Reference Signals (CRS)

The CRS are used for CSI estimation and demodulation purposes. They are transmitted in all downlink sub-frames (each 1ms) supporting PDSCH transmission and are defined for up to four antenna ports [38]. Depending on the antenna configuration, the CRS pattern and overhead can vary. For example, Figure 2 depicts the CRS configuration for a 2×2 MIMO system, where eight Resource Elements (RE) per transmit antenna per PRB are used. The yellow marked REs indicate the transmitted pilots per antenna port.

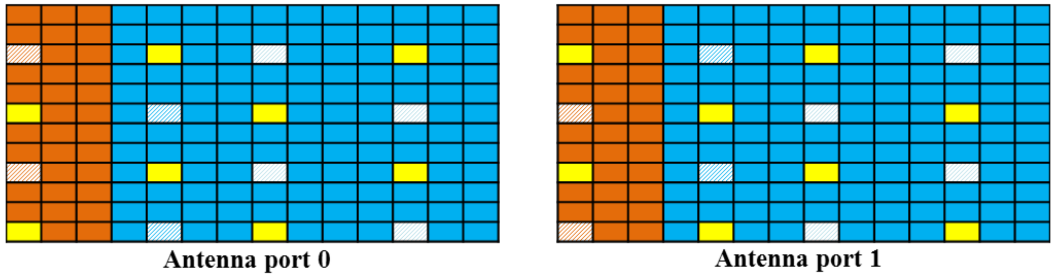

Figure 2: CRS reference signals for 2×2 MIMO

LTE-Advanced Release 10 support CRS backward compatibility for LTE legacy terminals.

CSI Reference Signals (CSI-RS)

The CSI-RS reference symbols are used in LTE-Advanced only for CSI measurements. These signals have lower frequency density and overhead compared with CRS and can be configured for transmission each 5ms, 10ms, 20ms, 40ms, or 80ms. CSI-RS patterns are defined for 1, 2, 4 and 8 transmit antennas and are based on TDM/CDM principles. There are 10 CSI-RS reuse patterns which allow cells to use different patterns and avoid mutual CSI-RS collisions [40].

Figure 3 depicts in purple color the CSI-RS pilots in a PRB grid. The same figure depicts the positions where the CRS pilots would be if configured. The yellow marked RE indicate the CRS transmitted for the antenna port 0.

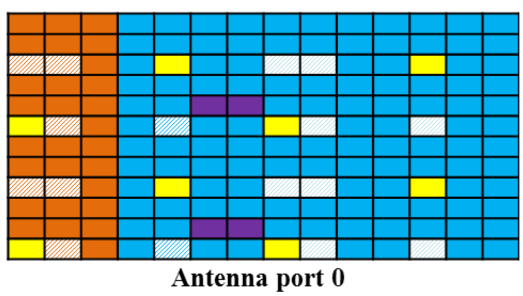

Figure 3: CSI-RS for a typical 4×2 MIMO configuration

UE-Specific Demodulation Reference Signals (DMRS)

The DMRS are UE-specific precoded pilots used for data demodulation. They are transmitted only on PRBs allocated for each UE's data and are precoded with the same precoder used for data transmission. DMRS allows channel estimation for demodulation to be performed per layer for up to eight transmission layers, thus the DMRS overhead depends only on the transmission rank. The DMRS overhead is 12 RE per PRB for ranks 1 and rank 2, and 24 RE for rank>2 [40]. A hybrid code division multiplexing (CDM) and frequency division multiplexing (FDM) scheme was adopted as a DMRS multiplexing scheme. The time domain "Orthogonal Cover Code" (OCC) is used for CDM since time domain orthogonality among OCCs is relatively robust against channel variation [41]. Figure 4 depicts an exemplary configuration for UE-specific reference signals having 12 RE. The DMRS pilots are marked in black color.

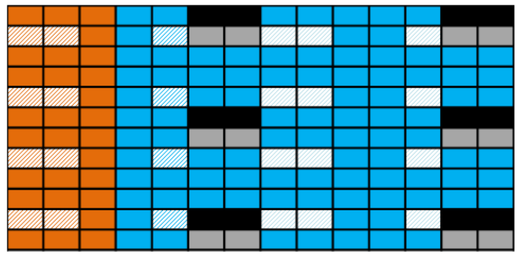

Figure 4: DMRS exemplary configuration

2.1.5 Transmission modes

There are nine Transmission Modes (TM) defined for LTE-Advanced out of which seven are defined in LTE Release 8, the eighth in Release 9 and the ninth in Release 10 [42]. The nine transmission modes are heavily based on Multiple-Input and Multiple-Output (MIMO) antenna techniques. One of the advantages MIMO techniques bring to LTE is the possibility to make simultaneous transmissions on the same time-frequency resources. These simultaneous transmissions are called transmission streams or transmission layers of a MIMO transmission.

The LTE-Advanced TM modes are:

- TM1 - Single-antenna transmission: In this mode the data is transmitted only by one antenna.
- TM2 - Transmit diversity: In this mode, the same information is transmitted on multiple antennas using Space-Frequency Block Codes (SFBC) which is an open-loop diversity technique. Only Channel Quality Indicator (CQI) information is required from the UE side.
- TM3 - Large delay CDD (Open-loop spatial multiplexing): Precoded transmission is used in this mode over two or more transmit antennas. As multiple code-words are used, this scheme provides better peak throughput than transmit diversity. This mode requires the UE to transmit only the transmit rank indicator to assign the number of code-words.
- TM4 - Closed-loop spatial multiplexing: In this mode the UE feeds back the Precoding Matrix Indicator (PMI) and Transmit Rank Indicator (RI) obtained from CRS reference signals. The closed-loop operation allows the transmitter to precode the data into orthogonal streams (maximum 4) as explained in Section 2.2.1. The used precoder matrix is signaled to the UE in the PDCCH.

- TM5 - Multi-user MIMO: This is a Rank 1 MU-MIMO transmission mode which is based on the same precoders and feedback information as TM4.
- TM6 - Closed-loop Rank 1 with pre-coding: This mode is similar to TM4 except that only one transmission stream is used.
- TM7 - Single antenna transmission: This mode is suitable for UE-specific beam-forming which makes use of the angle of arrival information (not closed-loop PMI feedback). The CQI is fed back with the time of arrival assumption.
- TM8 - Single or dual-layer transmission with UE-specific RS: This mode is a beam-forming mode which supports up-to 2 transmission layers. Closed-loop feedback based on UE-specific RS might or might not be used.
- TM9 - Closed-loop spatial multiplexing: This is a very flexible transmission mode where CSI-RS and UE-specific reference signals are used. This mode supports SU-MIMO with a maximum of eight transmission streams. Also, MU-MIMO [43] is supported in this mode.

2.2 MIMO antenna technology in LTE-Advanced

This section introduces the signal model used throughout this thesis. The first part introduces the basic concepts of a closed-loop “Multiple-Input Multiple-Output antenna” (MIMO) transmission, and the second part focuses on a more realistic system model applicable to LTE-Advanced.

2.2.1 Ideal closed-loop MIMO transmission

A MIMO system is composed by N_t transmit antennas and N_r receiver antennas, for simplicity we assume $N_\mathrm{t} \geq N_\mathrm{r}$. The MIMO channel matrix is defined as $\boldsymbol{H}$ with dimensions $N_\mathrm{r} \times N_\mathrm{t}$. The MIMO channel may be singular value decomposed (SVD) into at most N_r parallel non-interfering sub-channels as (see e.g [44])

$$\boldsymbol{H} \;=\; \boldsymbol{U}\boldsymbol{\Sigma}\boldsymbol{V}^\mathrm{H}, \tag{1}$$

where $\boldsymbol{U}$ is a $N_\mathrm{r} \times N_\mathrm{r}$ unitary matrix, $\boldsymbol{\Sigma}$ is a $N_\mathrm{r} \times N_\mathrm{t}$ matrix with N_r singular values of the channel on the main diagonal and $\boldsymbol{V}$ is a $N_\mathrm{t} \times N_\mathrm{t}$ unitary matrix. The number of the real positive singular values of the MIMO matrix is equal to the number of parallel non-interfering sub-channels available. This number also corresponds to the rank of the MIMO channel matrix. The parallel non-interfering sub-channels are also called transmission layers.

In a closed-loop MIMO transmission, the receiver feeds back the Channel State Information (CSI) of the channel. Using the CSI, the transmitter adapts the transmitted signal to the channel in order to maximize the link capacity. For a single-user transmission, with perfect knowledge of the channel at the transmitter end, the capacity can be maximized by adapting the transmitted signal to the channel with a precoder $\boldsymbol{W} = \boldsymbol{S}$, where $\boldsymbol{S}$ contains “r” columns of $\boldsymbol{V}$. The number of transmission layers is equal to the rank "r" of the MIMO channel. Similarly, the receiver filter will be $\boldsymbol{G}^{\mathrm{H}} = \boldsymbol{D}^{\mathrm{H}}$ where $\boldsymbol{D}$ contains "r" columns of $\boldsymbol{U}$. With an ideal precoder and receiver filter, the received signal

$$\underset{N_{\mathrm{r}}\times 1}{\boldsymbol{y}} = \underset{N_{\mathrm{r}}\times N_{\mathrm{t}}}{\boldsymbol{H}} \underset{N_{\mathrm{t}}\times \mathrm{r}}{\boldsymbol{W}} \underset{\mathrm{r}\times 1}{\boldsymbol{x}} + \underset{N_{\mathrm{r}}\times 1}{\boldsymbol{n}},$$

is filtered as

$$\begin{aligned} \boldsymbol{z} &= \boldsymbol{G}^{\mathrm{H}}\ \boldsymbol{y}, \\ &= \boldsymbol{G}^{\mathrm{H}}\ \boldsymbol{H}\ \boldsymbol{W}\ \boldsymbol{x} + \boldsymbol{G}^{\mathrm{H}}\boldsymbol{n}, \\ &= \boldsymbol{\Sigma}\ \boldsymbol{x} + \boldsymbol{D}^{\mathrm{H}}\ \boldsymbol{n}, \end{aligned} \tag{2}$$

and the signal model becomes diagonal [44].

2.2.2 System model for LTE-Advanced MIMO transmission

Taking into consideration that LTE-Advanced downlink makes use of OFDM modulation, where the transmitted sub-carriers are orthogonal by definition [34], it is enough to consider the received signal on a single sub-carrier. Moreover, the use of cyclic prefix will ensure that the inter-symbol interference is eliminated if the CP duration is longer than the delay spread of the multipath components. Assuming this is the case, it is enough to consider the received signal after the Fast-Fourier Transform (FFT) operation.

The system model is built by considering the center-cell of an LTE-Advanced cellular system. N_{eNB} is the number of eNBs in the system, and N_{u} are the number of users to be served, each user equipment has $N_{\mathrm{r}} = 2$ receiver antennas. The number of transmit antennas in all eNBs in the system is N_{t}. Furthermore, an eNB can simultaneously transmit to K UEs. In order to simplify the notation, the frequency domain sub-carrier index f_{sc} and time domain index t are omitted. The received signal vector $\boldsymbol{y}_{\mathrm{k}}$ by the k:th UE can be written as

$$\boldsymbol{y}_k = \boldsymbol{H}_{k,0}\ \boldsymbol{W}_k \boldsymbol{x}_k + \sum_{j=1}^{N_{\mathrm{eNB}}-1} \boldsymbol{H}_{k,j}\ \boldsymbol{W}_j \boldsymbol{x}_j + \boldsymbol{n}_{\mathrm{W},k}, \tag{3}$$

where $\boldsymbol{H}_{k,0}$ is the $N_r \times N_t$ MIMO channel matrix between the serving eNB and the k:th UE, $\boldsymbol{H}_{k,j}$ is the MIMO channel between the k:th UE and the j:th interfering eNB, $N_{\mathrm{eNB}} - 1$ indicates the number of interfering eNBs, and $\boldsymbol{n}_{\mathrm{W},k}$ is the noise vector whose entries are i.i.d. complex Gaussian distributed with zero mean and variance σ^2. The linear preprocessing matrices are $\boldsymbol{W}_k = [\boldsymbol{w}_{k,1}, ..., \boldsymbol{w}_{k,r}]$ where r is the transmission rank for the served k:th UE which indicates the number of transmission layers. Similarly, the transmitted signal vector $\boldsymbol{x}_k = \left[x_{k,1}^{\mathrm{H}}, ..., x_{k,r}^{\mathrm{H}}\right]^{\mathrm{H}}$ consists of r signals each transmitted per transmission layer. It is assumed that $\mathrm{E}(\boldsymbol{x}_{\mathrm{k}}\boldsymbol{x}_{\mathrm{k}}^{\mathrm{H}}) = \mathbf{I}$ and the total transmission power is controlled by conditioning $\mathrm{Tr}(\boldsymbol{W}_{\mathrm{k}}^{\mathrm{H}}\boldsymbol{W}_{\mathrm{k}}) = 1$. Finally, $\boldsymbol{W}_j$ and $\boldsymbol{x}_j$ are the preprocessing matrix and signal vector that the interfering eNBj uses for transmission in the analyzed time-frequency snapshot [23, 24, 43]. Equation (3) shows the three elements of our received signal, the desired received signal, the received interference and the received AWGN noise.

In order to further abstract our reference model, we define co-layer interference as the co-channel interference a transmission layer experiences due to other transmission layers transmitted from the same serving-eNB. For example, by focusing our attention in the first transmission layer and considering $r = 2$, we can write

$$\boldsymbol{y}_{k,1} = \boldsymbol{H}_{k,0}\ \boldsymbol{w}_{k,1} x_{k,1} + \boldsymbol{H}_{k,0}\ \boldsymbol{w}_{k,2} x_{k,2} + \sum_{j=1}^{N_{\text{eNB}}-1} \boldsymbol{H}_{k,j}\ \boldsymbol{W}_j \boldsymbol{x}_j + \boldsymbol{n}_{\text{W},k}, \tag{4}$$

and thus we can abstract our reference model as

$$\boldsymbol{y}_{k,1} = \ \boldsymbol{H}_{\text{eff},k}\ x_{k,1}\ +\ \boldsymbol{n}_{\text{c},k}, \tag{5}$$

where

$$\boldsymbol{H}_{\text{eff},k} = \boldsymbol{H}_{k,0}\ \boldsymbol{w}_{k,1}, \tag{6}$$

is the effective channel matrix of the first desired layer between the serving eNB and the k:th UE, and

$$\boldsymbol{n}_{\text{c},k} = \ \boldsymbol{H}_{k,0}\ \boldsymbol{w}_{k,2} x_{k,2} + \sum_{j=1}^{N_{\text{eNB}}-1} \boldsymbol{H}_{k,j}\ \boldsymbol{W}_j \boldsymbol{x}_j + \boldsymbol{n}_{\text{W},k} \tag{7}$$

is the colored noise vector formed by adding together the co-layer and inter-cell interference vectors with the AWGN noise vector. In addition, the co-layer effective channel matrix is defined as

$$\boldsymbol{H}_{\text{eff cl},k} = \boldsymbol{H}_{k,0}\ \boldsymbol{w}_{k,2}. \tag{8}$$

In contrast to the first part of this section, perfect knowledge of the CSI is not assumed anymore at the transmitter end, because in real life deployments only a limited capacity feedback channel is available [45]. The CSI is composed by the Channel Quality Indicator (CQI), the Precoder Matrix Indicator (PMI) and the Rank Indicator (RI). The CQI aids in the decision of which Modulation and Coding Scheme (MCS) the transmitter will use for downlink transmission. The PMI indicates the precoding matrix $\boldsymbol{W}$ to be used for single user transmission and it is chosen from a limited size codebook. The codebook used in this thesis is the LTE Release 8 codebook. The RI indicates the number of layers to be transmitted to a given UE.

In order to extract the desired signal $\boldsymbol{x}_k$, the received signal $\boldsymbol{y}_k$ is filtered by a receiver filter $\boldsymbol{G}_k^{\text{H}}$ as shown in (2). As the result, the post-processing received signal $\boldsymbol{z}_k$ is

$$\underset{\text{r}\times 1}{\boldsymbol{z}_k} = \underset{r\times N_r}{\boldsymbol{G}_k^{\text{H}}}\ \underset{N_r\times 1}{\boldsymbol{y}_k}\ . \tag{9}$$

It is possible to use different linear receiver filters. The ideal linear receiver that maximized the SINR when colored noise is present is the IRC receiver. A more detailed description about different linear receivers is given in Chapter 3.

2.3 Summary of differences between LTE and LTE-Advanced

LTE-Advanced is an evolution of LTE and as such many differences between them exist. From the point of view of this thesis, the main difference is the type of reference signals. LTE Release 8 was build around CRS reference signals. Channel State Information (CSI) measurements and channel estimation for demodulation used CRS signals. LTE-Advanced is built around a different model where CSI-RS reference signals are used for CSI measurements and UE-specific demodulation reference signals (DMRS) are used for demodulation of received layers.

3 Advanced linear interference aware receivers

In the LTE-Advanced standardization work performed by 3GPP, realistic modeling of linear MIMO receivers was deemed important [46, 47, 48] because advanced linear interference aware receivers can suppress a part of intra-cell and inter-cell interference improving downlink system performance. The improvement of LTE-Advanced downlink performance provided by IRC-type receivers at the UE side has been reported in for example in [22, 23, 24].

Linear interference suppression receivers have been studied in academic literature [4, 6, 7]. Initially, they were proposed for GSM uplink systems [8, 9, 10, 11, 12] and later for WCDMA High-Speed Downlink Packet Access (HSDPA) systems [18, 19, 20].

As this thesis focuses on modeling and evaluation of linear interference aware receivers for LTE-Advanced downlink, an introduction of the ideal linear receiver (IRC) is presented in this chapter. It follows a classification of different baseline linear receiver filters typically used by 3GPP and continues with the description and proposed modeling of advanced linear interference aware receivers which are possible implementations of the IRC.

Using techniques applicable for LTE-Advanced, especially its reference symbols and channel estimation structure, possible implementations of the IRC receiver have been proposed. Two different IRC receiver implementations are showed for example in [21, 22, 23, 24, 47] where the performance analysis is carried out with link level simulators.

In order to build a receiver filter based on the MMSE principle, an UE has to estimate the received interference covariance matrix. Well-known baseline linear receiver filters algorithms used by 3GPP RAN1/RAN4 groups are the MRC described in Section 3.2, the MRC with per-antenna noise suppression ($\mathrm{MRC_{PA}}$) described in Section 3.3, the LMMSE with co-layer interference suppression ($\mathrm{LMMSE_{CL}}$) described in Section 3.4. As will be seen later, the $\mathrm{LMMSE_{CL}}$ can at most suppress the co-layer intra-site interference if the desired received layer and the interfering co-layer originate from the same serving-eNB. In order to suppress interference originating from other-than-the-serving-eNBs, estimation of the inter-site interference covariance matrix is needed. In Section 3.5 and Section 3.6, two ways of estimating the interference covariance matrix are shown based on received data samples and reference symbols respectively. The system level modeling of these advanced linear aware receivers based on random matrix theory is also discussed.

3.1 Interference Rejection Combining (IRC)

The ideal optimum linear receiver for a closed-loop MIMO system can be found by using the Minimum Mean Square Error (MMSE) principle. In our particular case, and utilizing the system model presented in Section 2.2.2, the ideal linear receiver may suppress a part of the received interference if the covariance matrices of existing effective channels between the UE and all transmitting eNBs are completely known by the receiver.

This optimum receiver is also known in the literature as the optimum combiner or Interference Rejection Combiner (IRC) receiver. The IRC receiver has been extensively studied in many research articles since it was shown in [4] that it has superior performance compared with the Maximum Ratio Combiner (MRC) receiver when the interference experienced by each receiver antenna is correlated which is the case for deployed radio cellular networks with MIMO systems. However, the IRC receiver assumes the complete knowledge of all channel matrices which is an ideal assumption that cannot be met in deployed cellular systems due limited signaling and processing capabilities of user terminals. For this reason, the IRC receiver performance can be considered as the upper-limit of any linear receiver implementation based on the MMSE principle.

As a starting point in the analysis of advanced linear interference aware receivers, let us begin introducing the IRC [44]. Keeping in mind the signal model presented in Section 2.2 and Equation (9), it is known that one metric for evaluating the performance of the receiver filter $\boldsymbol{G}_k^{\mathrm{H}}$ is the mean square error [49] written as

$$E_{\mathrm{MSE}} \;=\; E\left[\|\, \boldsymbol{x}_k \;-\; \boldsymbol{G}_k^{\mathrm{H}} \boldsymbol{y}_k \,\|^2\right]. \tag{10}$$

Furthermore, combining Equations (5) and (10), and expanding the result leads to

$$E_{\mathrm{MSE}} \; = 1 - {\boldsymbol{H}_{\mathrm{eff}}}_k^{\mathrm{H}}\, \boldsymbol{G}_k^{\mathrm{H}} - \boldsymbol{G}_k\, {\boldsymbol{H}_{\mathrm{eff}}}_k \; + \boldsymbol{G}_k \left({\boldsymbol{H}_{\mathrm{eff}}}_k\, {\boldsymbol{H}_{\mathrm{eff}}}_k^{\mathrm{H}} + \boldsymbol{C}_{\mathrm{N}}\right) \boldsymbol{G}_k^{\mathrm{H}},$$

where $\boldsymbol{C}_{\mathrm{N}} = {\boldsymbol{n}^{\mathrm{H}}}_k\, \boldsymbol{n}_k$ is the covariance matrix of the colored noise which contains the intra-site (co-layer) and inter-site interference spatial signatures plus AWGN covariance. Calculating the gradient and looking for the minimum leads to the well-known linear minimum square error filter which can be expressed as

$$\boldsymbol{G}_k = {\boldsymbol{H}_{\mathrm{eff}}}_k^{\mathrm{H}} \left({\boldsymbol{H}_{\mathrm{eff}}}_k {\boldsymbol{H}_{\mathrm{eff}}}_k^{\mathrm{H}} + \boldsymbol{C}_{\mathrm{N}}\right)^{-1}, \tag{11}$$

where, ${\boldsymbol{H}_{\mathrm{eff}}}_k$ represents the effective channel of the desired signal intended to a given UE. Equation (11) can be also expressed as,

$$\boldsymbol{G}_k = {\boldsymbol{H}_{\mathrm{eff}}}_k^{\mathrm{H}} \left(\boldsymbol{C}_{\mathrm{rr}}\right)^{-1}, \tag{12}$$

where

$$\boldsymbol{C}_{\mathrm{rr}} = {\boldsymbol{H}_{\mathrm{eff}}}_k {\boldsymbol{H}_{\mathrm{eff}}}_k^{\mathrm{H}} + \boldsymbol{C}_{\mathrm{N}} \tag{13}$$

represents the complete received signal covariance. Different algorithms that estimate the total received covariance exist and their performance will be compared in Chapter 6.

In addition, the MIMO channel matrix between a given eNB and UE can be estimated from reference signals. Assuming the knowledge of the estimated channel matrices between the serving-eNB and a given UE the IRC can be written as

$$\hat{\boldsymbol{G}}_k = {\hat{\boldsymbol{H}}_{\mathrm{eff}}}_k^{\mathrm{H}} \left({\hat{\boldsymbol{H}}_{\mathrm{eff}}}_k {\hat{\boldsymbol{H}}_{\mathrm{eff}}}_k^{\mathrm{H}} + \hat{\boldsymbol{C}}_{\mathrm{N}}\right)^{-1}. \tag{14}$$

In order to analyze the receivers presented in the following sub-sections, it is useful to expand the colored noise covariance matrices $\boldsymbol{C}_{\mathrm{N}}$ and $\hat{\boldsymbol{C}}_{\mathrm{N}}$ as

$$\boldsymbol{C}_{\mathrm{N}} = \boldsymbol{C}_{\mathrm{CL}} + \boldsymbol{C}_{\mathrm{ext}} + \boldsymbol{C}_{\mathrm{W}}, \tag{15}$$

$$\hat{\boldsymbol{C}}_{\mathrm{N}} = \hat{\boldsymbol{C}}_{\mathrm{CL}} + \boldsymbol{C}_{\mathrm{ext}} + \boldsymbol{C}_{\mathrm{W}}. \tag{16}$$

The co-layer (CL) interference is produced by a co-scheduled transmission originating from the same serving-eNB as previously explained in Section 2.2.2. The covariance matrices for the interfering co-layer effective channel, Equation (8), and the interfering co-layer estimated effective channel are

$$\boldsymbol{C}_{\mathrm{CL}} = \boldsymbol{H}_{\mathrm{eff\,cl,k}} \boldsymbol{H}_{\mathrm{eff\,cl,k}}{}^{\mathrm{H}}, \tag{17}$$

$$\hat{\boldsymbol{C}}_{\mathrm{CL}} = \hat{\boldsymbol{H}}_{\mathrm{eff\,cl,k}} \hat{\boldsymbol{H}}_{\mathrm{eff\,cl,k}}{}^{\mathrm{H}}. \tag{18}$$

The inter-cell interference covariance matrix is the sum of all interference covariance matrices experienced between a given UE and $N_{\mathrm{eNB}} - 1$ interfering eNBs on a given time-frequency resource. When the ideal knowledge of the MIMO channel matrices is assumed, the inter-cell interference covariance matrix reads

$$\boldsymbol{C}_{\mathrm{ext}} = \sum_{j=1}^{N_{\mathrm{eNB}}-1} \boldsymbol{H}_{\mathrm{eff,ext}_j} \boldsymbol{H}_{\mathrm{eff,ext}_j}{}^{\mathrm{H}}, \tag{19}$$

and the average white Gaussian noise covariance matrix is a diagonal matrix whose diagonal elements contain the experienced AWGN noise powers

$$\boldsymbol{C}_{\mathrm{W}} = \mathrm{diag}(\sigma_1, \cdots, \sigma_i), \tag{20}$$

where each received antenna is assumed to experience the same AWGN noise power, $\sigma_i = \sigma$, $\forall i$.

3.2 Maximum Radio Combining (MRC)

The white-noise approximation of the MRC receiver is defined as

$$\boldsymbol{G}_k = \boldsymbol{H}_{\mathrm{eff}\,k}^{\mathrm{H}}, \tag{21}$$

and after considering channel estimation, the MRC is

$$\hat{\boldsymbol{G}}_k = \hat{\boldsymbol{H}}_{\mathrm{eff}\,k}^{\mathrm{H}}. \tag{22}$$

It can be noticed that the white-noise approximated MRC does not take into consideration the experienced colored noise as the IRC receiver does. Furthermore, MRC requires minimum knowledge of the radio environment as it needs only the desired layer channel coefficients. The MRC has lower performance on correlated channels compared with the IRC. [4, 6].

3.3 MRC with per-antenna noise suppression ($\mathrm{MRC_{PA}}$)

The 3GPP option 1 receiver [46] is considered a baseline linear receiver used in LTE-Advanced standardization by 3GPP members. The $\mathrm{MRC_{PA}}$ assumes that each receiver antenna knows the received colored noise-plus-interference power and the algorithm requires only the effective channel's covariance matrix of the desired layer. Other possible co-scheduled transmitted layers from the same serving-eNB (sharing the same PRBs) intended, or not, for the same UE are not estimated. For a single-user system, with rank > 1, this means that only the covariance matrix of the layer to be decoded is estimated. The complete co-layer interference covariance matrix is assumed not known, however some information is included in the colored noise covariance term. The $\mathrm{MRC_{PA}}$ receiver filter can be written as

$$\boldsymbol{G}_k = \boldsymbol{H}_{\mathrm{eff}\,k}^{\mathrm{H}} \left(\boldsymbol{H}_{\mathrm{eff}\,k}\ \boldsymbol{H}_{\mathrm{eff}\,k}{}^{\mathrm{H}} + \ \mathrm{diag}\left(\boldsymbol{C}_{\mathrm{N}}\right)\right)^{-1}, \tag{23}$$

and after considering channel estimation, the $\mathrm{MRC_{PA}}$ can be rewritten as

$$\hat{\boldsymbol{G}}_k = \hat{\boldsymbol{H}}_{\mathrm{eff}\,k}^{\mathrm{H}} \left(\hat{\boldsymbol{H}}_{\mathrm{eff}\,k}\ \hat{\boldsymbol{H}}_{\mathrm{eff}\,k}{}^{\mathrm{H}} + \ \mathrm{diag}\left(\boldsymbol{C}_{\mathrm{N}}\right)\right)^{-1}. \tag{24}$$

The colored noise covariance matrix is considered to diagonal, where

$$\mathrm{diag}\left(\boldsymbol{C}_{\mathrm{N}}\right) = \mathrm{diag}(\sigma_1, \cdots, \sigma_i), \tag{25}$$

is the diagonal part. It is assumed that each received antenna experience colored noise power, $\sigma_i \neq \sigma_j$, $\forall i, j$, $i \neq j$. Hence, no spatial information about the interferers is included in the receiver filter.

3.4 LMMSE with co-layer interference suppression ($\mathrm{LMMSE_{CL}}$)

The $\mathrm{LMMSE_{CL}}$, also called 3GPP option 2, is the second baseline linear receiver used by 3GPP members. The main difference between $\mathrm{MRC_{PA}}$ and $\mathrm{LMMSE_{CL}}$ receivers is that $\mathrm{LMMSE_{CL}}$ estimates covariance matrices for all desired layers. In other words, the co-layer interference generated in single user transmissions with rank>1 is taken into account by the receiver filter. The $\mathrm{LMMSE_{CL}}$ receiver filter can be written as

$$\boldsymbol{G}_k = \boldsymbol{H}_{\mathrm{eff}\,k}^{\mathrm{H}} \left(\boldsymbol{H}_{\mathrm{eff}\,k}\ \boldsymbol{H}_{\mathrm{eff}\,k}{}^{\mathrm{H}} + \ \boldsymbol{H}_{\mathrm{eff\,cl}k}\boldsymbol{H}_{\mathrm{eff\,cl}k}{}^{\mathrm{H}} + \ \mathrm{diag}\left(\boldsymbol{C}_{\mathrm{nn}}\right)\right)^{-1}, \tag{26}$$

and after considering channel estimation, it can be rewritten as

$$\hat{\boldsymbol{G}}_k = \hat{\boldsymbol{H}}_{\mathrm{eff}\,k}^{\mathrm{H}} \left(\hat{\boldsymbol{H}}_{\mathrm{eff}\,k}\ \hat{\boldsymbol{H}}_{\mathrm{eff}\,k}{}^{\mathrm{H}} + \ \hat{\boldsymbol{H}}_{\mathrm{eff\,cl}k}\hat{\boldsymbol{H}}_{\mathrm{eff\,cl}k}{}^{\mathrm{H}} + \ \mathrm{diag}\left(\boldsymbol{C}_{\mathrm{nn}}\right)\right)^{-1}, \tag{27}$$

where $\mathrm{diag}\left(\boldsymbol{C}_{\mathrm{nn}}\right)$ represents the colored noise for this receiver filter. The covariance matrix $\boldsymbol{C}_{\mathrm{nn}}$ is formed by the inter-site interference covariance matrix and the AWGN noise covariance as

$$\boldsymbol{C}_{\mathrm{nn}} = \ \boldsymbol{C}_{\mathrm{ext}} + \boldsymbol{C}_{\mathrm{W}}.$$

Generally speaking, LMMSE_{CL} has a better performance than MRC_{PA} because it estimates effective channels for all transmitted layers between the serving-eNB and a given UE. This approach effectively reduces intra-cell interference, improving especially average cell throughput (as shown in Section 6).

In order to reduce the inter-cell interference (interference coming from other transmission points than the serving-eNB), the knowledge of the external interference covariance matrix is needed. Direct estimation of effective channels between a given UE and its strongest external interferers and later calculation of the external interference covariance matrices would be desirable, but it is not possible in the current LTE-Advanced system because of signaling and processing time restrictions. Thus, a different approach based on the indirect estimation of external interference covariance matrices is used [21, 22, 22, 23, 47, 48].

In the following sections two algorithms that indirectly estimate the IRC interference covariance matrix are presented, the first estimates the total covariance matrix needed by the IRC receiver using the received data symbols, the second indirectly estimates the external interference covariance matrix using reference symbols.

3.5 Data-sample-based linear interference aware receiver ($\text{LMMSE-IRC}_{\text{WI-DATA}}$)

The data-sample-based linear interference aware receiver is an IRC receiver in which the IRC interference covariance matrix is estimated using received data samples. In this section, the data-sample-based IRC interference covariance matrix estimation algorithm will be shown and after the Wishart distribution based emulation of the IRC interference covariance matrix estimation will be presented. The acronym $\text{LMMSE-IRC}_{\text{WI-DATA}}$ indicates the Wishart distribution based emulation of the data-sample-based linear interference aware receiver.

The covariance matrix used by the IRC receiver can be computed with an algorithm that utilizes the received data samples to estimate the whole received signal covariance matrix $\hat{\boldsymbol{C}}_{\text{rr}}$. In this case, the desired and interfering signal covariance matrices are not estimated independently, but a single estimate is computed which includes the spatial information about the desired and interfering signals [21, 22, 23, 24, 47, 48].

The data-sample-based interference aware receiver utilizes the estimated covariance matrix $\hat{\boldsymbol{C}}_{\text{rr}}$ for building the receiver filter in a similar way as the IRC in Equation (12). The received signal covariance matrix can be estimated using received data samples as

$$\begin{aligned}\hat{\boldsymbol{C}}_{\text{rr}} &= \frac{1}{N_{\text{DS}}}\sum_{n=1}^{N_{\text{DS}}}\boldsymbol{r}_n\boldsymbol{r}_n{}^{\text{H}} \\ &= \frac{1}{N_{\text{DS}}}\boldsymbol{R}\boldsymbol{R}^{\text{H}},\end{aligned} \tag{28}$$

where, N_{DS} indicates the number of data samples considered,
$\boldsymbol{R} = \begin{bmatrix} \boldsymbol{r}_1 & \boldsymbol{r}_2 & \cdots & \boldsymbol{r}_n & \cdots & \boldsymbol{r}_{N_{\mathrm{DS}}} \end{bmatrix}$ is a matrix which has N_{DS} columns and $\boldsymbol{r}_n$ has dimensions $N_{\mathrm{r}} \times 1$. Note that all columns of $\boldsymbol{R}$ are independent. The received vector sample $\boldsymbol{r}_n$ is formed by data samples taken from the same position in time and frequency domain on each receiver antenna. The vector $\boldsymbol{r}$ is assumed to be a p-variate random variable with covariance $\boldsymbol{C}_{\mathrm{rr}}$. The estimate is created as the average of N_{DS} sample covariance matrices of individual received vector samples. The received modulated samples can be chosen randomly from the PDSCH received modulated symbols in time and frequency [48]. The estimated spatial covariance matrix contains the directional knowledge of the intended signal and interference signals. An IRC-type receiver could be implemented directly with this algorithm without additional channel estimation capabilities. However, in a system simulator the actual received baseband samples are not available as explained in Section 1.2, thus a model is needed to study the potential receiver gain in different scenarios of interest.

The emulation of the covariance matrix estimation is possible thanks to the tools developed in random matrix theory. As shown in Annex A.4, the sample covariance matrix follows a Wishart distribution with N_{DS} degrees of freedom and covariance matrix $\boldsymbol{C}_{\mathrm{rr}}$ if the columns $\boldsymbol{r}_n$ of the sample vector are complex Gaussian distributed.

$$\frac{1}{N_{\mathrm{DS}}} \sum_{n=1}^{N_{\mathrm{DS}}} \boldsymbol{r}_n \boldsymbol{r}_n^{\mathrm{H}} \sim \mathrm{W}\left(N_{\mathrm{DS}}, \boldsymbol{C}_{\mathrm{rr}}\right)$$

$$\hat{\boldsymbol{C}}_{\mathrm{rr}} \sim \mathrm{W}\left(N_{\mathrm{DS}}, \boldsymbol{C}_{\mathrm{rr}}\right).$$

The Wishart distribution allows us to generate with N_{DS} degrees of freedom an estimated covariance matrix $\hat{\boldsymbol{C}}_{\mathrm{rr}}$ which has similar statistical properties as the ideal covariance matrix $\boldsymbol{C}_{\mathrm{rr}}$. The Bartlett's decomposition (see Annex A.5) easies the computation of the estimated covariance matrix $\hat{\boldsymbol{C}}_{\mathrm{rr}}$ by allowing

$$\hat{\boldsymbol{C}}_{\mathrm{rr}} \approx \boldsymbol{L}\boldsymbol{A}\boldsymbol{A}^{\mathrm{H}}\boldsymbol{L}^{\mathrm{H}}, \tag{29}$$

where the lower triangular matrix $\boldsymbol{L}$ can be computed numerically using the Cholesky decomposition $\boldsymbol{C}_{\mathrm{rr}} = \boldsymbol{L}\boldsymbol{L}^{\mathrm{H}}$. The diagonal elements of the $N_{\mathrm{r}} \times N_{\mathrm{r}}$ $\boldsymbol{A}$ lower triangular matrix follow a Chi-square distribution such that $c_{ii} = a_{ii}^2$, $c_{ii} \sim \mathcal{X}^2_{N_{\mathrm{DS}}-i+1}$ $(i = 1, \ldots, N_{\mathrm{r}})$, with independent elements a_{ij} $(1 \leq j \leq i \leq N_{\mathrm{r}})$ following a normal distribution $\mathcal{N}(0,1)$ and elements a_{ij} $(1 \leq i \leq j \leq N_{\mathrm{r}})$ equal zero [50], in other words matrix $\boldsymbol{A}$ can be expressed as

$$\boldsymbol{A} = \begin{bmatrix} \sqrt{c_{11}} & 0 & \cdots & \cdots & 0 \\ n_{2,1} & \sqrt{c_{22}} & 0 & \cdots & 0 \\ n_{3,1} & n_{3,2} & \sqrt{c_{33}} & \cdots & 0 \\ \vdots & \vdots & \vdots & \ddots & 0 \\ n_{N_{\mathrm{r}},1} & n_{N_{\mathrm{r}},2} & \cdots & \cdots & \sqrt{c_{N_{\mathrm{r}}N_{\mathrm{r}}}} \end{bmatrix}. \tag{30}$$

The number of data samples N_{DS} taken into account varies according the subframe configuration due to the number of OFDM symbols assigned for PDCCH, and antenna configuration due to the overhead caused by reference signals as briefly explained in Section 2.1.4. For example, assuming 3 ODFM symbols reserved for PDCCH and 4×2 antenna configuration where DMRS are used (12 RE overhead) then $N_{\mathrm{DS}} = (14 - 3) \times 12 - 12 = 120$. Finally, the data-sample-based linear interference aware receiver considering channel estimation is

$$\hat{\boldsymbol{G}}_k = \hat{\boldsymbol{H}}_{\mathrm{eff}\,k}^{\mathrm{H}} \left(\hat{\boldsymbol{C}}_{\mathrm{rr}} \right)^{-1}, \tag{31}$$

where $\hat{\boldsymbol{C}}_{\mathrm{rr}}$, can be computed with Equation (29), with N_{DS} degrees of freedom.

This Wishart distribution based modeling has been used in an LTE-Advanced system simulator to evaluate the performance of the data-sample-based interference aware receiver. Furthermore, during the research period the Wishart distribution based modeling has been validated in different publications [23, 47, 48] against an actual data-sample-based IRC receiver that uses baseband samples for the computation of the covariance matrix in a link level simulator.

3.6 Reference-symbol-based linear interference aware receiver (LMMSE-IRC$_{\mathrm{WI\text{-}RS}}$)

The reference-symbol-based linear interference aware receiver is an IRC receiver in which the IRC external interference covariance matrix is estimated using reference symbols or pilots. In this section, the external interference covariance matrix estimation algorithm will be shown and after the Wishart distribution based emulation of the IRC external interference covariance matrix estimation will be presented. The acronym LMMSE-IRC$_{\mathrm{WI\text{-}RS}}$ indicates the Wishart distribution based emulation of the reference-symbol-based linear interference aware receiver.

The LMMSE-IRC$_{\mathrm{WI\text{-}RS}}$ receiver algorithm utilizes an external interference covariance matrix estimated indirectly using reference symbols transmitted on the PDSCH. In this receiver, the covariance matrix is divided into two parts, the intracell interference covariance matrix and the external interference covariance matrix. As shown below, both covariance matrices can be calculated using reference symbols. Moreover, the receiver filter will look like the LMMSE$_{\mathrm{CL}}$ in Equation (27) except for the additional external covariance matrix term $\boldsymbol{C}_{\mathrm{ext}}$. Considering channel estimation the receiver filter reads

$$\hat{\boldsymbol{G}}_k = \hat{\boldsymbol{H}}_{\mathrm{eff}\,k}^{\mathrm{H}} \left(\hat{\boldsymbol{H}}_{\mathrm{eff}\,k}\, \hat{\boldsymbol{H}}_{\mathrm{eff}\,k}^{\mathrm{H}} + \hat{\boldsymbol{H}}_{\mathrm{eff\,cl}k} \hat{\boldsymbol{H}}_{\mathrm{eff\,cl}k}^{\mathrm{H}} + \hat{\boldsymbol{C}}_{\mathrm{ext}} + \boldsymbol{C}_{\mathrm{W}} \right)^{-1}, \tag{32}$$

where the inter-cell interference covariance matrix $\hat{\boldsymbol{C}}_{\mathrm{ext}}$ is estimated from the residual information on the reference symbol (RS) positions as

$$\hat{\boldsymbol{C}}_{\mathrm{ext}} = \frac{1}{N_{\mathrm{RS}}} \sum_{n=1}^{N_{\mathrm{RS}}} \boldsymbol{s}_n \boldsymbol{s}_n^{\mathrm{H}}, \tag{33}$$

where N_{RS} is the number of reference symbols available on the PDSCH, n corresponds to a specific time-frequency location on the analyzed PRB where reference symbols are located and $\boldsymbol{s}_n$ is the residual interference vector. The residual interference vector is defined as

$$\boldsymbol{s}_n = \boldsymbol{y}_n - \hat{\boldsymbol{H}}_{\mathrm{eff}\,n}\boldsymbol{p}_n, \tag{34}$$

where $\boldsymbol{y}_n$ is the received signal vector in the n time-frequency position, $\hat{\boldsymbol{H}}_{\mathrm{eff}\,n}$ is the estimated effective channel in the n time-frequency position and $\boldsymbol{p}_n$ is the transmitted reference symbol vector on the n time-frequency position. The external interference covariance matrix can be also expressed as

$$\begin{aligned}\hat{\boldsymbol{C}}_{\mathrm{ext}} &= \frac{1}{N_{\mathrm{RS}}}\sum_{n=1}^{N_{\mathrm{RS}}}\boldsymbol{s}_n\boldsymbol{s}_n^{\mathrm{H}} \\ &= \frac{1}{N_{\mathrm{RS}}}\sum_{n=1}^{N_{\mathrm{RS}}}\left(\boldsymbol{y}_n - \hat{\boldsymbol{H}}_{\mathrm{eff}\,n}\boldsymbol{p}_n\right)\left(\boldsymbol{y}_n - \hat{\boldsymbol{H}}_{\mathrm{eff}\,n}\boldsymbol{p}_n\right)^{\mathrm{H}}.\end{aligned} \tag{35}$$

The RS-based linear interference aware receiver needs the actual baseband signals and reference symbols for the external interference noise covariance estimation. The reference-symbol-based linear interference aware receiver can also be emulated using the Wishart distribution as the data-based linear interference aware receiver was emulated.

The emulation of the IRC external interference covariance matrix is performed as follows. The external interference covariance matrix follows a Wishart distribution with N_{RS} degrees of freedom and covariance matrix $\boldsymbol{C}_{\mathrm{ext}}$ defined in Equation (19), such that

$$\hat{\boldsymbol{C}}_{\mathrm{ext}} \sim \mathrm{W}\left(N_{\mathrm{RS}}, \boldsymbol{C}_{\mathrm{ext}}\right), \tag{36}$$

The computation of the emulated external interference covariance matrix can be performed with the Bartlett's decomposition as discussed in the previous section. This emulation will be used in the LTE system simulator to assess the performance of RS-based interference aware receivers. The external interference covariance matrix can also be expressed as

$$\begin{aligned}\boldsymbol{C}_{\mathrm{ext}} &= \mathrm{E}\left[\left(\boldsymbol{y}_n - \hat{\boldsymbol{H}}_{\mathrm{eff}\,n}\boldsymbol{p}_n\right)\left(\boldsymbol{y}_n - \hat{\boldsymbol{H}}_{\mathrm{eff}\,n}\boldsymbol{p}_n\right)^{\mathrm{H}}\right] \\ &= \mathrm{E}\left[\left(\boldsymbol{y}_n - (\boldsymbol{H}_{\mathrm{eff}\,n} + \boldsymbol{\epsilon}_n)\boldsymbol{p}_n\right)\left(\boldsymbol{y}_n - (\boldsymbol{H}_{\mathrm{eff}\,n} + \boldsymbol{\epsilon}_n)\boldsymbol{p}_n\right)^{\mathrm{H}}\right] \\ &= \boldsymbol{C}_{\mathrm{rr}} - \boldsymbol{H}_{\mathrm{eff}\,n}\boldsymbol{H}_{\mathrm{eff}\,n}^{\mathrm{H}} + \boldsymbol{C}_{\epsilon},\end{aligned} \tag{37}$$

where $\hat{\boldsymbol{H}}_{\mathrm{eff}\,n} = (\boldsymbol{H}_{\mathrm{eff}\,n} + \boldsymbol{\epsilon}_n)$ indicates that the estimated effective channel can be modeled with an error matrix $\boldsymbol{\epsilon}_n$ [23, 47]. It is assumed that the channel estimation error $\boldsymbol{\epsilon}_n$ is uncorrelated from the received RS symbols $\boldsymbol{y}_n$ in order to simplify the model. The channel estimate is obtained through filtering the same symbol set, which actually means that depending on the channel estimation filter and assumed interference and noise level, the estimation noise could in fact be correlated between the samples which are sampled from the frequency and time domains. Considering that relatively good quality channel estimates are made, the magnitude of the diagonal elements of $\boldsymbol{C}_\epsilon$ should be relatively small compared with the total interference power. Thus, further simplification of Equation (37) could be assumed in the modeling resulting in

$$\boldsymbol{C}_{\text{ext}} = \boldsymbol{C}_{\text{rr}} - \boldsymbol{H}_{\text{eff}\,n}\boldsymbol{H}_{\text{eff}\,n}^{\text{H}}. \tag{38}$$

As mentioned in Section 2.1.4, LTE makes use of two types of reference symbols to acquire CSI information and perform channel estimation for demodulation. The correct configuration of reference symbols depends on the transmission mode (see Section 2.1.5). The transmission modes of interest are TM4 and TM9 because they use closed-loop MIMO and multi-rank transmission. TM4 is based on CRS and TM9 is based on CSI-RS and DMRS. The reference-symbol-based interference aware receiver might have different implementations depending if CRS or DMRS is used for demodulation, but the modeling in system level is rather similar as explained later.

3.6.1 Cell-specific-RS-based linear interference aware receiver

LTE Release 8 defines the first seven LTE transmission modes based on CRS reference signals (Section 2.1.4). In case of having TM4 mode, CRS can be used to estimate the external interference covariance matrix by subtracting the transmitted CRS symbols affected by the estimated effective channel from the received CRS symbols in a specific time/frequency position. The estimated effective channel is the estimated channel multiplied by the used precoder at the receiver side. This provides the estimated interference amplitude seen by data symbols. The external interference covariance is computed as

$$\begin{aligned}
\hat{\boldsymbol{C}}_{\text{CRS}} &= \frac{1}{N_{\text{CRS}}}\sum_{n=1}^{N_{\text{CRS}}} \boldsymbol{s}_n\boldsymbol{s}_n^{\text{H}} && (39)\\
&= \frac{1}{N_{\text{CRS}}}\sum_{n=1}^{N_{\text{CRS}}} \left(\boldsymbol{y}_n - \hat{\boldsymbol{H}}_{\text{eff}\,n}\boldsymbol{p}_n\right)\left(\boldsymbol{y}_n - \hat{\boldsymbol{H}}_{\text{eff}\,n}\boldsymbol{p}_n\right)^{\text{H}} && (40)\\
&= \frac{1}{N_{\text{CRS}}}\sum_{n=1}^{N_{\text{CRS}}} \left(\boldsymbol{y}_n - \hat{\boldsymbol{H}}_n\boldsymbol{w}\boldsymbol{p}_n\right)\left(\boldsymbol{y}_n - \hat{\boldsymbol{H}}_n\boldsymbol{w}\boldsymbol{p}_n\right)^{\text{H}} && (41)
\end{aligned}$$

where $\boldsymbol{w}$ is the precoder utilized for the data transmission in the layer to be decoded and studied PRB, the vector $\boldsymbol{y}_n$ contains the received CRS symbols and the vector $\boldsymbol{p}_n$ contains the transmitted CRS symbols.

As explained in Equation (36), the external interference covariance matrix estimation algorithm based on CRS can be emulated using the Wishart distribution as

$$\hat{\boldsymbol{C}}_{\text{CRS}} \sim \text{W}\left(N_{\text{CRS}}, \boldsymbol{C}_{\text{ext}}\right), \tag{42}$$

where the number of CRS reference symbols in the PDSCH equals N_{CRS}. For example, a 2×2 MIMO antenna configuration is configured with 16 CRS per PRB out of which 12 CRS are located in the PDSCH. The receiver filter can be computed as

$$\hat{\boldsymbol{G}}_k = \hat{\boldsymbol{H}}_{\mathrm{eff}\,k}^{\ \ \mathrm{H}} \left(\hat{\boldsymbol{H}}_{\mathrm{eff}\,k} \hat{\boldsymbol{H}}_{\mathrm{eff}\,k}^{\ \ \mathrm{H}} + \hat{\boldsymbol{H}}_{\mathrm{eff\,cl}k} \hat{\boldsymbol{H}}_{\mathrm{eff\,cl}k}^{\ \ \mathrm{H}} + \hat{\boldsymbol{C}}_{\mathrm{CRS}} + \boldsymbol{C}_{\mathrm{W}} \right)^{-1}. \tag{43}$$

This emulation will be used in a system simulator to assess the performance of CRS-based interference aware receivers.

3.6.2 UE-specific-RS based linear interference aware receiver

LTE-Advanced Release 10 and forthcoming releases can make use of CSI-RS and DMRS reference signals as previously explained in Section 2.1.4. In case of having TM9 mode, the UE-specific demodulation reference symbols (DMRS) can also be used to estimate the external interference covariance matrix by subtracting the transmitted DMRS symbol affected by the estimated effective channel from the actual received DMRS symbols in a specific time/frequency position. This provides the estimated external interference amplitude. We compute the external interference covariance as

$$\begin{aligned} \hat{\boldsymbol{C}}_{\mathrm{DMRS}} &= \frac{1}{N_{\mathrm{DMRS}}} \sum_{n=1}^{N_{\mathrm{DMRS}}} \boldsymbol{s}_n \boldsymbol{s}_n^{\ \mathrm{H}} \\ &= \frac{1}{N_{\mathrm{DMRS}}} \sum_{n=1}^{N_{\mathrm{DMRS}}} \left(\boldsymbol{y}_n - \hat{\boldsymbol{H}}_{\mathrm{eff}\,n} \boldsymbol{p}_n \right) \left(\boldsymbol{y}_n - \hat{\boldsymbol{H}}_{\mathrm{eff}\,n} \boldsymbol{p}_n \right)^{\mathrm{H}} \end{aligned} \tag{44}$$

where the vector $\boldsymbol{y}_n$ contains the received DMRS symbols and vector $\boldsymbol{p}_n$ contains the DMRS transmitted symbols from the serving-eNB for the time-frequency position n [23, 24, 47]. As explained in Equation (36), the DMRS based external interference covariance matrix estimation algorithm can be emulated using the Wishart distribution as

$$\hat{\boldsymbol{C}}_{\mathrm{DMRS}} \sim \mathrm{W}\left(N_{\mathrm{DMRS}}, \boldsymbol{C}_{\mathrm{ext}} \right), \tag{45}$$

where N_{DMRS} equal to the configured number of DMRS symbols. For example, a 4×2 MIMO is configured with 12 DMRS per PRB. The receiver filter can be computed as

$$\hat{\boldsymbol{G}}_k = \boldsymbol{H}_{\mathrm{eff}\,k}^{\mathrm{H}} \left(\boldsymbol{H}_{\mathrm{eff}\,k} \boldsymbol{H}_{\mathrm{eff}\,k}^{\ \ \mathrm{H}} + \boldsymbol{H}_{\mathrm{eff\,cl}k} \boldsymbol{H}_{\mathrm{eff\,cl}k}^{\ \ \mathrm{H}} + \hat{\boldsymbol{C}}_{\mathrm{DMRS}} + \boldsymbol{C}_{\mathrm{W}} \right)^{-1}. \tag{46}$$

This emulation will be used in a system simulator to assess the performance of DMRS-based interference aware receivers.

4 Simulation model

A radio network is a complex system that can be modeled with different levels of abstraction depending on the problem to be studied. After a system is properly modeled, computer simulations can be performed. A popular method of performing computer simulations is by utilizing Monte Carlo methods.

Monte Carlo methods form an experimental branch of mathematics that employs simulations driven by random number generators [51]. In a very general manner, Monte Carlo experiments can be categorized in two broad classes: 1) Direct simulation of a naturally random system; and 2)Addition of artificial randomness to a system. In the context of radio network simulations, the natural randomness of fading processes of the channel is considered in the simulator according to the specific channel models used (See Section 4.3). Also, the distribution of UEs and small-cells in the simulator follow a random process as will be explained in Sections 4.1 and 4.2.

An accurate performance analysis of a radio network in terms of transmission chain, baseband processing, scheduling processing, radio channel modeling, network topology, network traffic, etc is computationally prohibitive. Thus, it is common to perform the analysis from either a system level perspective or a link level perspective in order to reduce computational complexity.

System level simulators are designed to model more realistic interference environments by including multiple cells, multiple UEs and special channel models like the Spatial Channel Model (SCM) or ITU-R channel models. In system level simulators a large radio network can be studied. On the other hand, system level simulators lack of baseband signal modeling which make the study of advanced receiver algorithms very challenging. In contrast, link level simulators model a point-to-point transmission chain in detail but lack of realistic interference modeling.

System level simulators of radio systems can be classified in 3 groups: static, quasi-static and dynamic system level simulators. In a static simulator, mobile terminals do not change positions during simulation time, hence the radio environment in terms of fast fading stays invariable during simulation time. In a dynamic simulator, mobile terminals change positions during simulation time, hence the path-loss and fast-fading values of mobile terminals are changing during simulation time. The quasi-static simulator provides a complexity compromise between static and dynamic simulators. In a quasi-static simulator, mobile terminals do not change positions during simulation time (path-loss remains the same), but the fast-fading is emulated by assigning a speed parameter to the mobile terminal. In this thesis, a quasi-static simulator is utilized for all the presented simulations.

This thesis makes use of an LTE-Advanced system level model. In the model, the proper link details are simplified such as the minimum time domain granularity is one sub-frame (1ms). Thus, proper OFDM symbols are not modeled and instead of performing the demodulation process with baseband signals, a Link-to-System interface is used to map SINR values to throughput values via look-up BER tables [52]. Also, the traffic process is modeled as a full buffer model. This model assumes that all UEs in the network have data waiting to be transmitted all the time. Furthermore, the scheduler is modeled as a proportional fair scheduler in both time and frequency domains as explained in [53].

Traditionally, in order to assess the exact performance of linear receiver algorithms, link level analysis is performed using actual baseband signals. However, link level analysis tends to overlook the complex interference structure experienced by UEs located in different geographical positions in a multi-cell environment. On the other hand, system level analysis takes into account complex interference structures but the study of linear receiver algorithms is challenging due to the lack of baseband signals.

4.1 Network topology

In order to provide a wider view on the performance of linear receiver algorithms, five different network topologies, which include homogeneous and heterogeneous networks, have been considered in this thesis. The macro (homogeneous) topology is characterized by an hexagonal layout composed by 19 sites, each site hosting three macro eNBs (MeNB), or 3 sectors. All MeNBs transmit with the same transmission power. The heterogeneous topology is an extension of the macro topology where small-cells (e.g. pico-cells) are dropped within the MeNB's region of coverage. The main characteristics of the heterogeneous topology are that pico-eNBs (PeNB) have an omni-directional antenna pattern and transmit with reduced power compared with a MeNB. The specific assumptions for the different topologies can be found in Table 1.

Table 1: Assumptions about network topologies

Network topologies	Simulation assumptions
Macro 3GPP Case 1	See Table 3
Macro 3GPP Case 3	See Table 3
Macro ITU-R UMa	See Table 4
Heterogeneous network Configuration 1	See Tables 4 and 5
Heterogeneous network Configuration 4b	See Tables 4 and 5

4.2 User equipment distribution

The UE distribution depends on the network topology. For homogeneous topologies, it is assumed that 10 UEs are uniformly distributed inside each sector. This means that at the beginning of a simulation run, random experiments are performed where UEs are dropped into the network with (x, y) coordinates, where "x" and "y" follow uniform distributions. After 10 UEs are successfully dropped inside each simulated MeNB region of coverage, the simulation starts. After a large number of simulation runs are performed, the results are averaged in order to obtain a clear picture of the performance for a given network topology.

In case of heterogeneous topologies, two UE dropping modes are considered: Heterogeneous network Configuration 1 and Configuration 4b. Both configurations include sectors having one MeNB and four uniformly distributed PeNB within the sector. Configuration 1 is a non-clustered UE dropping mode, where 25 UEs are uniformly distributed inside a sector. In contrast, Configuration 4b is a clustered UE dropping mode where 10 UEs are uniformly distributed inside a sector, following the same rules as in the homogeneous topology, and 5 UEs are uniformly distributed inside each PeNB region of coverage. The final cell selection between UEs and radio stations (MeNB or PeNB) is performed by received power levels.

Table 2 summarizes the UE distributions across the scenarios of interest considered in this thesis.

Table 2: Distribution of UEs across the scenarios

Scenario	Macro eNB	Pico eNB
3GPP Case 1	10 UE uniformly distributed	-
3GPP Case 3	10 UE uniformly distributed	-
ITU-R UMa	10 UE uniformly distributed	-
HetNet Configuration 1	30 UE uniformly distributed in macro coverage region	
HetNet Configuration 4b	10 UE uniformly distributed in macro coverage region	5 UE uniformly distributed in pico coverage region

4.3 Channel models

The channel model describes the characteristics of the wireless channel to be studied. These characteristics can be described in terms of path-loss, shadowing, multi-path components, Doppler spread and fast-fading. The channel models considered in this thesis are the models utilized by 3GPP members in the development of LTE-Advanced standards. The selection of the correct channel model will depend of the scenario of interest. Generally speaking, two main channel models are considered: the 3GPP channel models, and the ITU-R channel models.

The 3GPP Spacial Channel Models (SCM) used in this thesis are Case 1 and Case 3 [54, 55]. Case 1 represents a dense urban deployment scenario where Inter-Site Distance (ISD) is 500m with 15° of electrical antenna tilt, and Case 3 represents a deployment where ISD is 1732m with 6° of electrical antenna tilt. Also, SCM models the required elements to study the effects MIMO antenna technologies.

Furthermore, the ITU-R has approved ITU-R channel models for the evaluation of IMT-A systems [56]. In this thesis, the Urban Macrocell (UMa) and Urban Microcell (UMi) models are used for the macro ITU-R UMa deployment and the heterogeneous deployments.

The simulation assumptions for different channel models together with corresponding network topologies can be referred from Table 1.

Table 3: Simulation assumptions for 3GPP macro Case 1 and 3

Parameters	**Case 1**	**Case 3**
Bandwidth	10 MHz	
Carrier frequency	2000 MHz	
Cellular layout	Hexagonal grid, 19 cell sites, 3 sectors per site	
Inter-site distance	500m	1732m
Distance dependent path-loss	$L = 128.1 + 37.6 \log_{10}(R)$ R: Km	
Shadowing standard deviation	8 dB	
Shadowing correlation: Between cells Between sectors	- 0.5 1.0	
Penetration loss	20 dB	
Antenna pattern horizontal	$A_{\mathrm{H}}(\varphi) = -\min\left[12\left(\frac{\varphi}{\varphi_{\mathrm{3dB}}}\right)^2, A_{\mathrm{m}}\right]$ $\varphi_{\mathrm{3dB}} = 70°$ degrees, $A_{\mathrm{m}} = 25$ dB	
Antenna pattern vertical	. $A_{\mathrm{V}}(\theta) = -\min\left[12\left(\frac{\theta - \theta_{\mathrm{etilt}}}{\theta_{\mathrm{3dB}}}\right)^2, SLA_{\mathrm{v}}\right]$ $\theta_{\mathrm{3dB}} = 10°$ degrees, $SLA_{\mathrm{v}} = 20$ dB Antenna height at the eNB is set to 32 m. Antenna height at the UE is set to 1.5 m.	
Antenna pattern vertical, electrical tilt	$\theta_{\mathrm{etilt}} = 15°$degree	$\theta_{\mathrm{etilt}} = 6°$degree
Combined 3D antenna pattern	$A(\varphi, \theta) = -\min\{-[A_{\mathrm{H}}(\varphi) + A_{\mathrm{V}}(\theta)], A_{\mathrm{m}}\}$	
Total eNB TX power (PTotal)	46 dBm	
Minimum distance between UE and Cell	≥ 35 meters	
Hard Handover hysteresis	ideal selection and 3 dB margin	
Traffic model	Full Buffer	
UEs/sector	10	
Other assumptions	See [54]	

Table 4: Simulation assumptions for ITU-R UMa

Parameters	**ITU-R UMa**
Type of user	Outdoor user
Bandwidth	10 MHz
Carrier frequency	2000 MHz
Cellular layout	Hexagonal grid, 19 cell sites, 3 sectors per site
Inter-site distance	500m
Average street width	20m
Average building height	20m
Break point distance	$d_{\mathrm{BP}} = 4h_{\mathrm{BS}}h_{UT}f_{\mathrm{c}}/c$
Probability of LOS	$P_{\mathrm{LOS}} = \min(18/d, 1) \times (1 - \exp(-d/36) + \exp(-d/36)$ d : distance [m]
Path-loss LOS	For $10m < d < d_{BP}$, $L = 22.0\log(d) + 28.0 + 20\log(f_{\mathrm{c}})$ For $d_{\mathrm{BP}} < d < 5000m$, $L = 40\log(d) + 7.8 - 18.0\log(h_{\mathrm{BS}}) - 18.0\log(h_{\mathrm{UT}}) + 2.0\log(f_c)$
Path-loss NLOS	$L = 161.04 - 7.1\log(W) + 7.5\log(h) - (24.37 - 3.7(h/h_{\mathrm{BS}})^2)\log(h_{\mathrm{BS}}) + (43.42 - 3.1\log(h_{BS}))(\log(d) - 3) + 20\log(f_c) - (3.2(\log(11.75h_{\mathrm{UT}}))^2 - 4.97)$
Total eNB TX power (PTotal)	46 dBm
eNB noise figure	5 dB
UE noise figure	7 dB
eNB antenna gain (boresight)	17dBi
UE antenna gain	0dBi
Hard Handover hysteresis	Ideal selection and 3 dB margin
Traffic model	Full Buffer
UEs/sector	10
Other assumptions	See [54, 56]

Table 5: Simulation assumption for ITU-R UMi cases

Parameters	**ITU-R UMi**
Type of user	Outdoor user
Bandwidth	10 MHz
Carrier frequency	2000 MHz
Cellular layout	Small-cell below macro coverage region
Break point distance	$d_{\mathrm{BP}} = 4h_{\mathrm{BS}}h_{UT}f_{\mathrm{c}}/c$
Probability of LOS	$P_{\mathrm{LOS}} = \min(18/d, 1) \times (1 - \exp(-d/36) + \exp(-d/36)$ d : distance [m]
Path-loss LOS	For $10m < d < d_{BP}$, $L = 22.0\log(d) + 28.0 + 20\log(f_{\mathrm{c}})$ For $d_{\mathrm{BP}} < d < 5000m$, $L = 40\log(d) + 7.8 - 18.0\log(h_{\mathrm{BS}}) - 18.0\log(h_{\mathrm{UT}}) + 2.0\log(f_c)$
Path-loss NLOS	Valid for the hexagonal cell layout $L = 36.7\log(d) + 22.7 + 26\log(f_{\mathrm{c}})$
Total eNB TX power (PTotal)	30 dBm
Antenna pattern vertical	$A_{\mathrm{V}}(\theta) = -\min\left[12\left(\frac{\theta - \theta_{\mathrm{etilt}}}{\theta_{\mathrm{3dB}}}\right)^2, SLA_{\mathrm{v}}\right]$ $\theta_{\mathrm{3dB}} = 40^\circ$ degrees, $SLA_{\mathrm{v}} = 20$ dB
eNB noise figure	5 dB
UE noise figure	7 dB
eNB antenna gain (boresight)	17dBi
UE antenna gain	0dBi
Other assumptions	See [54, 56]

4.4 Antenna array configuration and antenna gain pattern

The spatial MIMO channel is dependent of the utilized antenna configuration [44, 56]. In this thesis, Uniform Linear Arrays (ULA) and Cross-polarized (XP) antenna arrays are considered. The ULA is a configuration where the N antenna elements are placed parallel to each other and separated by a distance d. Also, the antenna elements form a slant angle with respect to the horizon. The XP is a configuration where N antenna elements are placed in pairs forming a cross. Each pair is separated by a distance d. Also, the antenna pair form a slant angle with respect to the horizon.

The distance between the antenna elements (or pairs) is controlled by selecting a suitable distance d as a multiple of the wavelength (λ) of the carrier frequency. Closely spaced arrays make use of $d = \lambda/2$, whereas widely spaced arrays make use of $d = 4\lambda$. In addition, the correlation between the antenna elements can be controlled by selecting a suitable combination of distance d and antenna configuration. For example, a high correlation is obtained by using a closely spaced XP antenna configuration, and a low correlation is obtained by using a widely spaced ULA antenna configuration.

The antenna pattern gain is modeled as a 3D pattern. The 3D antenna gain pattern is built as a combination of horizontal and vertical antenna gains. The 3D antenna gain considers both the (x, y, z) UE position and the fixed electrical tilt of the eNB antenna array. For example, a description of the 3GPP Case 1 3D antenna pattern is given below. The 3GPP Case 1 antenna pattern model is defined in Table 6 and depicted in Figure 5. A 3-sector site is located at the center of the figure. Each sector is separated by 120°degrees, the eNB height is 32m, the electrical downtilt angle is 15°degrees and the UE height is 1.5m. The site mast is located on the z-axis, and Figure 5 provides a 2D view looking from the top of the mast to the ground. The red color indicates higher values of C/I while the dark blue color represents C/I $\leq$ -3dB.

The horizontal antenna pattern provides the horizontal antenna gain of the beam inside a sector. Near the sector edge, the gain might take the value of the minimum default -Am depending on the angle φ. Similarly, the vertical antenna pattern provides the vertical antenna gain. If an UE is too close or too far from the mast, the θ-angle can be such that the vertical antenna gain takes the minimum default value of - SLAv.

The 3D combination method also allows for a condition where the minimum default can be selected. Both situations are noticed when the minimum default values of gains are selected near the central circle in Figure 5, were the C/I value is -3dB (the antenna gains of three sectors yield the same value). This also happens on the outer area of the figure. This behavior is caused by the antenna model and might not exactly reflect real life antenna patterns.

During simulations, one avoids dropping UEs in the central area by adjusting the minimum UE - eNB distance, and the electrical tilt angle. The outer area receives coverage from other sites. It is worth repeating that the 3D antenna pattern utilizes a fixed eNB tilt for all simulated UEs because the antenna array is considered to be a passive antenna array. A passive antenna array is a traditional array where the

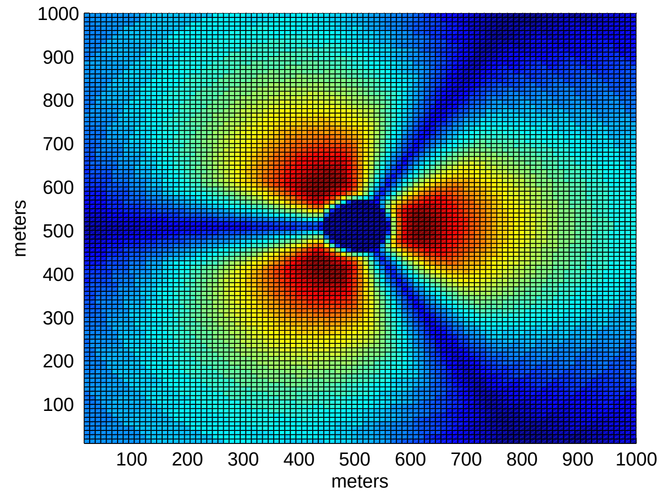

Figure 5: 3D pattern for antenna gain

Table 6: 3D antenna pattern for 3GPP macro Case 1

Parameter	**Value**
Antenna pattern horizontal	$A_{\mathrm{H}}(\varphi) = -\min\left[12\left(\frac{\varphi}{\varphi_{\ 3\mathrm{dB}}}\right)^2, A_{\mathrm{m}}\right]$ $\varphi_{\ 3\mathrm{dB}} = 70°$ degrees, $A_{\mathrm{m}} = 25$ dB
Antenna pattern vertical	$A_{\mathrm{V}}(\theta) = -\min\left[12\left(\frac{\theta - \theta_{\mathrm{etilt}}}{\theta_{\ 3\mathrm{dB}}}\right)^2, SLA_{\mathrm{v}}\right]$ $\theta_{\ 3\mathrm{dB}} = 10°$ degrees, $SLA_{\mathrm{v}} = 20$ dB Antenna height at the eNB is set to 32 m. Antenna height at the UE is set to 1.5 m. $\theta_{\ \mathrm{etilt}} = 15°$degree
Combined 3D antenna pattern	$A(\varphi, \theta) = -\min\{-[A_{\mathrm{H}}(\varphi) + A_{\mathrm{V}}(\theta)], A_{\mathrm{m}}\}$

power electronics are located outside the antenna array and the vertical antenna tilt is fixed. In contrast, in an active antenna array the power electronics are located within each antenna elements. One of the characteristics of active antenna array is that the antenna tilt can be variable for each transmission. This can enable a model where each simulated UE will use an optimized eNB tilt in order to improve C/I and reduce interference.

5 Interference analysis of the LTE-Advanced radio network

It was previously mentioned in the introduction that there is a belief that in many LTE deployment scenarios exist a dominant source of interference that can be rejected by using the Interference Rejection Combining receiver (IRC). The existence of a dominant source of interference is indeed analyzed in this chapter and shown using an LTE system level simulator.

The radio spectrum is a scarce resource that should be utilized as efficiently as possible. In order to achieve this goal, continuous enhancements in the radio link performance, advanced RRM methods and interference mitigation techniques are used. For example, the LTE-Advanced system uses frequency-reuse equal one meaning the whole available frequency band is reused by every eNB in the network. In practice, using the same frequency band in neighboring cells will cause high levels of inter-cell interference especially at cell edges.

In the next section, an introductory analysis of the interference situation experience by UEs inside an LTE-Advanced radio network is provided.

5.1 LTE-Advanced as interference-limited cellular system

It is well-known that the capacity of a densely deployed cellular system is interference limited. The Signal-to-Interference-plus-Noise ratio (SINR) is a metric for the desired signal quality that gives insight about the experienced interference situation. In an homogeneous cellular network composed by N_{eNB} Macro eNBs, the SINR in downlink direction, from the point of view of the UE_i and a single antenna, can be modeled as

$$\Gamma(i) = \frac{g_{ii}p_i BW}{\left(\sum\limits_{j=1;j\neq i}^{N_{eNB}} g_{ij}p_j\right) BW + \sigma^2\left(BW\right)} = \frac{g_{ii}p_i}{\sum\limits_{j=1;j\neq i}^{N_{eNB}} g_{ij}p_j + \sigma^2}, \tag{47}$$

where, g_{ii} is the link gain between the UE_i and the serving eNB_i, p_i(W/Hz) is the serving eNB transmission power per Hz, g_{ij} is the link gain between the UE_i and the interfering eNB_j, p_j(W/Hz) is the interfering eNB_j transmission power per Hz, BW(Hz) is the system bandwidth and σ^2(W/Hz) is the noise power density. Assuming that the interference power density is very much greater than the noise power density, that is $\sum\limits_{j=1;j\neq i}^{N_{eNB}} g_{ij}p_j \gg \sigma^2$, we can rewrite the SINR as

$$\Gamma(i) \approx \frac{g_{ii}p_i}{\sum\limits_{j=1;j\neq i}^{N_{eNB}} g_{ij}p_j}.$$

Furthermore, in a macro deployment all eNBs transmit with the same power $p_i = p_j$, thus the SINR can be further simplified as

$$\Gamma(i) \approx \frac{g_{ii}}{\sum_{j=1;j\neq i}^{N_{eNB}} g_{ij}}$$

From the latter expression, we can see that the SINR is independent of the transmit power, moreover the SINR is derived by the network topology and channel conditions. Maintaining the former assumptions the same conclusion can be obtained from (47), if $p_i \gg \sigma^2$ then $(\sigma^2/p_i) \to 0$ as

$$\Gamma(i) = \frac{g_{ii}}{\sum_{j=1;j\neq i}^{N_{eNB}} g_{ij} + \left(\frac{\sigma^2}{p_i}\right)} \approx \frac{g_{ii}}{\sum_{j=1;j\neq i}^{N_{eNB}} g_{ij}} \tag{48}$$

This SINR concept can easily be extended to the case where pico-eNBs (PeNB) are deployed within the macro coverage using frequency reuse one, that is the macro eNB (MeNB) and PeNBs share the same frequency band. Supposing that PeNB transmit power p_m is lower than MeNB transmit power p_i, that is $p_m = \alpha p_i$, thus from Equation (47) the SINR is

$$\begin{aligned}\Gamma(i) &= \frac{g_{ii} p_i BW}{\sum_{j=1;j\neq i}^{N_{eNB}} g_{ij} p_j BW + \sum_{m=1}^{N_{PeNB}} g_{im} p_m BW + \sigma^2 BW} \\ &= \frac{g_{ii} p_i}{\sum_{j=1;j\neq i}^{N_{eNB}} g_{ij} p_j + \sum_{m=1}^{N_{PeNB}} g_{im} p_m + \sigma^2},\end{aligned}$$

This yields the interference limited SINR as

$$\Gamma(i) \approx \frac{g_{ii}}{\sum_{j=1;j\neq i}^{N_{eNB}} g_{ij} + \alpha \sum_{m=1}^{N_{PeNB}} g_{im}}, \tag{49}$$

It is clear from Equations (48) (49) that the SINR values for a heterogeneous network are lower than for the macro case. This situation is worse at cell-edge where the external interference signal powers are strong and the serving cell signal power is weak. Nonetheless heterogeneous networks bring gains due to cell splitting [57].

5.2 Interference profile analysis

As explained in Section 2.1.3, the LTE-Advanced time/frequency resource is divided into physical resource blocks (PRBs) that are assigned to UEs by a time/frequency scheduler [53]. The scheduling decisions of neighboring cells will affect the instantaneous/short-term interference levels experienced by UEs.

In a full-buffer case study, it is safe to assume in the long-term that the interference originating from other-than-the-serving cells is present on the whole bandwidth regardless of the scheduling decisions. Hence, the interference profile characterization metric can be based only on the wideband received power level. A classic quality metric that characterizes the interference levels of a given network topology is the wideband SINR. In general, the wideband SINR, also called Geometry factor, can be written as

$$\Gamma = \frac{I_{\text{or}}}{I_{\text{oc}} + N} = \frac{S_0}{\sum_{i=1}^{M-1} S_i + N},$$

where, $M = N_{\text{eNB}} + N_{\text{PeNB}}$ indicates the number of eNBs present in the studied network, N is the noise power, S_i is a vector of received power levels, I_{oc} is the sum of received powers from all interfering eNBs which can be expanded as

$$I_{\text{oc}} = \sum_{i=1}^{M-1} S_i.$$

It is assumed that S_i is sorted by power intensity in descending order, except for the first element S_0 which correspond always to the serving-eNB received power, that is $I_{\text{or}} = S_0$. Moreover, note that the received power of the serving-eNB is never considered in any I_{oc} calculation as this term indicates exclusively interference power.

The contribution to the total interference differs from interferer to interferer mainly due to network topology and UE location. This thesis aims to analyze this variation utilizing an interference metric called Dominant Interference Proportion of the interferer j (DIP_j) which is a variation of the well-known Dominant to rest of Interference Ratio (DIR) [16]. The DIR_j is defined as

$$DIR_j = \frac{S_j}{\sum_{i=1, i\neq j}^{M-1} S_i + N}; \quad \forall j > 0,$$

and the Dominant Interference Proportion of the interferer j (DIP_j) is defined as

$$DIP_j = \frac{S_j}{\sum_{i=1}^{M-1} S_i + N}; \quad \forall j > 0, \tag{50}$$

and differs from the DIR_j only in the denominator term. The DIR_j is a ratio between the power of an interferer j to the rest of the interference plus noise power, and the DIP_j is a ratio between the power of an interferer j to the total interference plus noise power. Also note from Equation (50) that the SINR can be expressed as $\Gamma = DIP_0$. As S_i is assumed to be sorted by interference power strength, the DIP_1 indicates ratio of the power of the most dominant interferer to the total interference plus noise power in the system.

In addition, the DIP_j and DIR_j are related quantities. It is easy to show that

$$DIP_j = \frac{1}{\frac{1}{DIR_j} + 1} = \frac{DIR_j}{1 + DIR_j}.$$

For this reason, this thesis will use DIP_j to analyze via computer simulations interference profiles in different network topologies and deployment scenarios as its conversion to DIR_j is trivial.

As explained in Section 5.1, the sources of downlink interference in a macro radio network deployment are other macro-eNBs and the interference profile depends mainly on the macro network topology. Moreover, it will be shown in the following sub-sections that the interference profile also depends on the cell selection procedure, specifically on the hard hand-over margin value.

5.2.1 Homogeneous macro 3GPP Case 1

In this sub-section the interference profile for the 3GPP macro Case 1 will be study via computer simulations. The simulation model and assumptions were presented in Section 4 and in Section 4.1, Table 3 respectively. Other specific simulation assumptions are shown in Table 7.

Table 7: Additional simulation assumptions for interference profile assessment

Parameter	**Value**
Number of realizations	100 runs
Hard Hand-over margin	0 dB (ideal selection) and 3 dB
Traffic model	Full Buffer
UEs/sector	10

The interference profile for the studied homogeneous macro radio network deployment is mainly showed for two values of hard hand-over (HO) margin 0 dB (also called ideal cell selection) and 3 dB. The hard hand-over margin has an effect on the system geometry specially in the cell-edge zone as depicted Figure 6 for six HO margin values (0 dB, 2 dB, 3 dB, 4 dB, 5 dB and 6 dB). From the figure it is observed that the number of cell-edge terminals increases (the number of UE in low geometry zone increases) when a higher handover margin value is used compared with the ideal cell selection case. Different geometry distributions will affect the interference profile as shown later.

The DIP profile for the eight strongest interferers is computed for every simulated terminal. One simulation run includes 19 sites containing three macro-eNBs each, 10 UEs are dropped inside every eNB coverage area. Thus, the total number of UEs per run is $19 \times 3 \times 10 = 570$. In order to have a considerable high number of samples to compute meaningful statistics, one hundred runs have been simulated and some statistical measures have been computed on the sample pool.

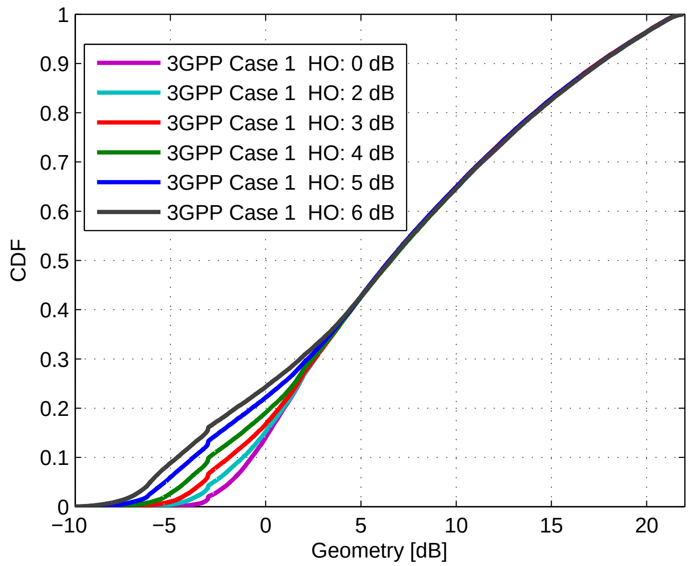

Figure 6: Geometry of the 3GPP Case 1 for selected values of hard hand-over margin

First statistics computed from the sample pool are unconditional median DIP_j of the eight strongest interferers. The name unconditional median comes from the fact that the median DIP_j is computed from all observations unconditionally of their geometry factor value. The resulting profiles $DIP_1, \cdots, DIP_8$ are presented in Figure 7 and Figure 8 as power ratios for the ideal cell selection and 3 dB handover margin cases respectively. Figure 7 and Figure 8 show that DIP values might be differentiable up-to DIP_5 , thereafter DIP values are very small.

It can be observed that indeed a dominant interference exists which contains almost 50% of the total interference power in this macro case. Also, Table 8 shows the cumulative sum of dominant interferers powers to the total interference where it is observed that the contribution of the most dominant 5 interferers correspond to more than 80% of the total interference power.

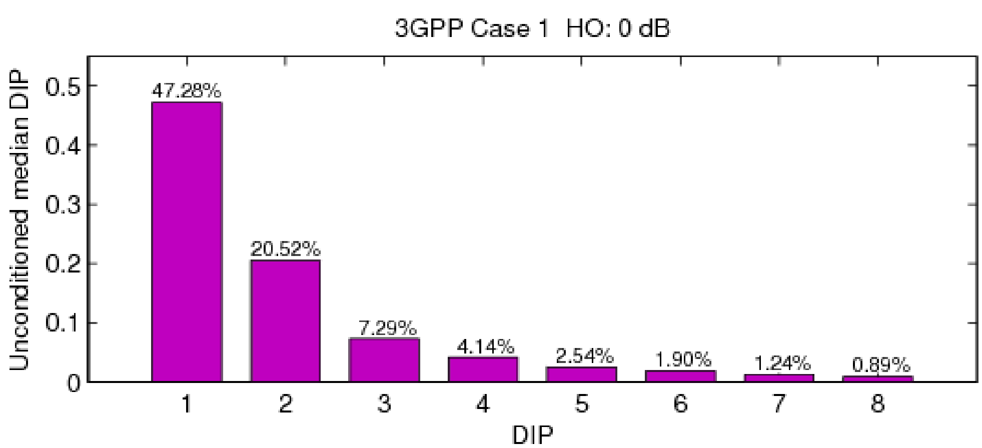

Figure 7: Unconditioned median DIP profile, 3GPP Case 1, ideal cell selection

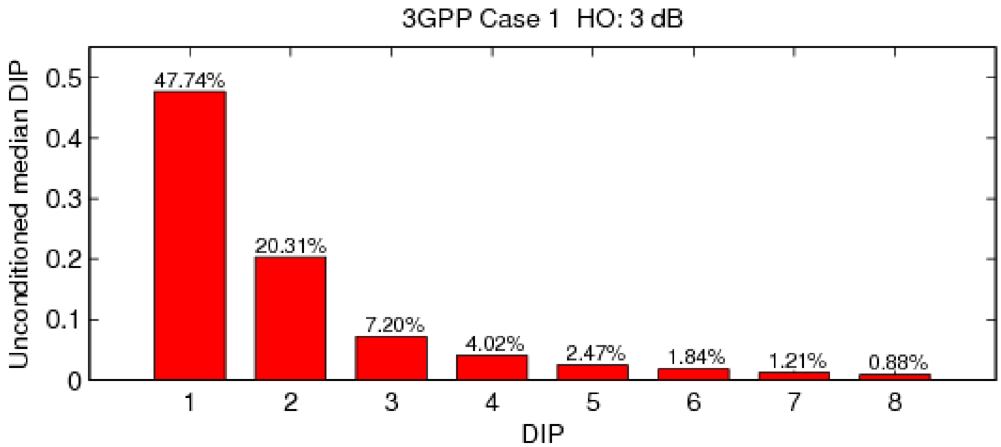

Figure 8: Unconditioned median DIP profile, 3GPP Case 1, HO margin 3 dB

Table 8: Cumulative sum of interference power from dominant interferers for 3GPP Case 1 deployment scenario

HO margin	DIP_1	DIP_2	DIP_3	DIP_4	DIP_5	DIP_6	DIP_7	DIP_8
0 dB	47.28%	20.52%	7.29%	4.14%	2.54%	1.90%	1.24%	0.89%
Cum. sum	47.3%	67.8%	75.1%	79.2%	81.8%	83.7%	84.9%	85.8%
3 dB	47.99%	20.23%	7.09%	3.91%	2.39%	1.78%	1.18%	0.86%
Cum. sum	48.0%	68.2%	75.3%	79.2%	81.6%	83.4%	84.6%	85.4%

It is unlikely that all UEs can be characterized by using only an unconditional median DIP profile. Interference profiles of UEs with high geometry value should be different compared with DIP profiles of UEs with low geometry value e.g. UEs located on the cell-edge. This means the unconditional median DIP might not be the most representative interference profile. In order to improve the interference analysis, the sample pool is divided into sub-sets based on a geometry condition plus a given tolerance, then the median DIP is computed for the selected sub-sets as explained below. This method is called conditional median DIP.

1. Choose a set of geometry values for which the analysis will be performed.

2. Create sample sub-sets by filtering UEs with the given geometry conditions considering a tolerance of ± 0.2 (e.g. $G = 0$ dB $\pm\, 0.2$ dB)

3. Collect the values inside the sub-set and compute the median DIP.

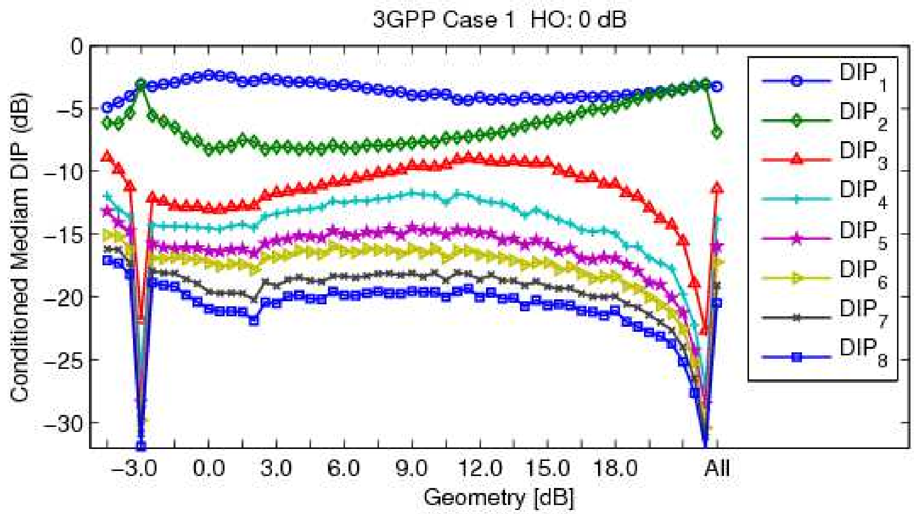

Figure 9: Conditioned median DIP profile [dB], 3GPP Case 1, ideal cell selection

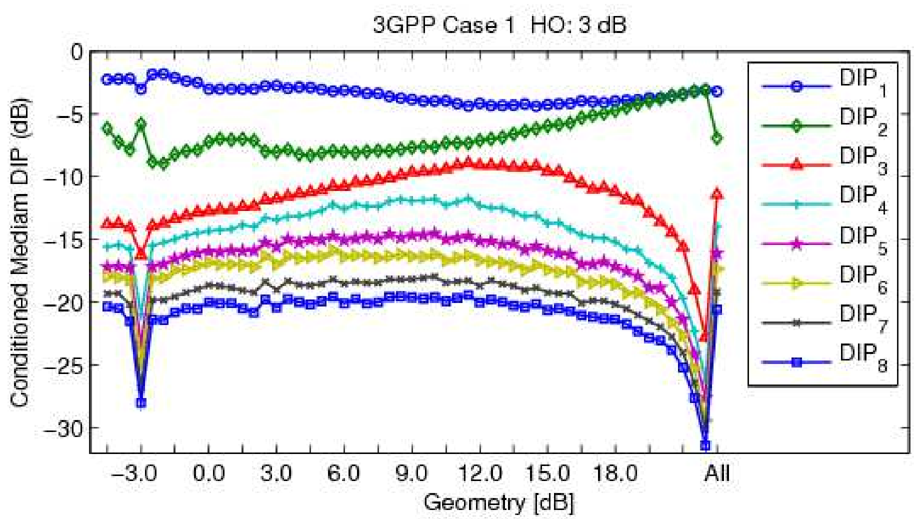

Figure 10: Conditioned median DIP profile [dB], 3GPP Case 1, HO = 3 dB

The conditional median DIP profiles computed for the ideal cell selection and cell selection with hard hand-over margin of 3 dB are depicted in Figure 9 and Figure 10 respectively for geometry points ranging from -4 dB to +22 dB with a 0.5 dB step. The depicted figures show how the DIP values change at different geometry positions. The label “All” in the mentioned tables refer to the unconditional DIP values. From the figures it is clearly observed that the power of the first dominant and second dominant interferers varies across the geometry axis. Nonetheless, in most of the geometry positions exists a clear dominant interferer.

In addition, a strange behavior its noticed exactly at the condition G = -3 dB for both simulated cases. Especially from Figure 10, it is observed that at G ≈ -3 dB, the $DIP_1 \approx DIP_2 \approx -3$ dB , which suggests that the serving cell and the two strongest interferer cells have almost same transmission power.

In order to better understand this behavior, the location map of simulated UEs having G ≈ -3 dB is depicted in Figure 11 for the cell selection with hand-over margin of 3 dB. The figure suggests there is a clustering of UEs near the eNB and on the border between sectors. After filtering the UE´s having $DIP_1 = -3 \pm 0.3$ dB, we can see in Figure 12 that indeed a clustering behavior is present under these conditions. This clustering behavior is an articraft caused by the 3GPP 3D antenna pattern used and does not reflect a real antenna pattern behavior, hence the DIP profile conditioned to G ≈ -3 dB should not be considered as representative of the macro case. The same observations have been found an described in [58, 59]. For comparison purposes another UE position map at geometry G ≈ -2.5dB is depicted in Figure 13. In Figure 13 the clustering behavior is not present.

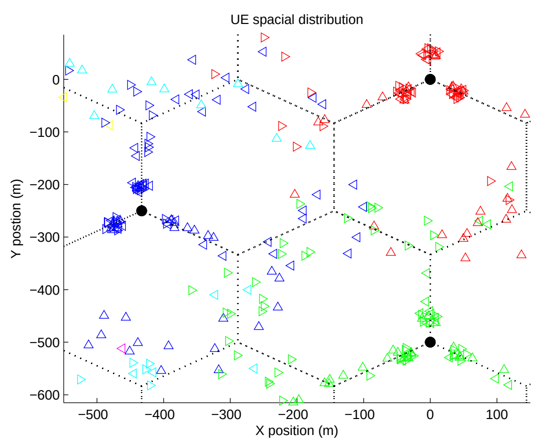

Figure 11: UE position map - Geometry ≈ -3dB

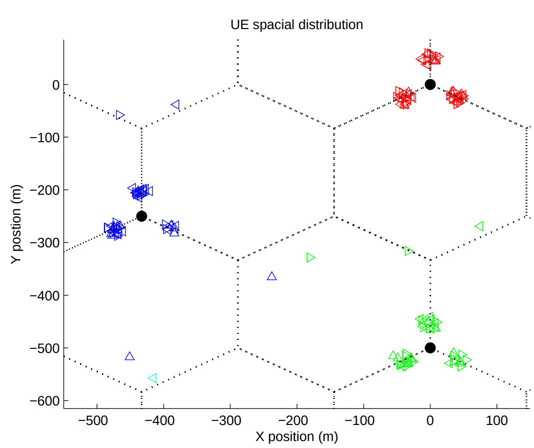

Figure 12: UE position map - Geometry ≈ -3dB & DIP_1 = -3 ±0.3dB

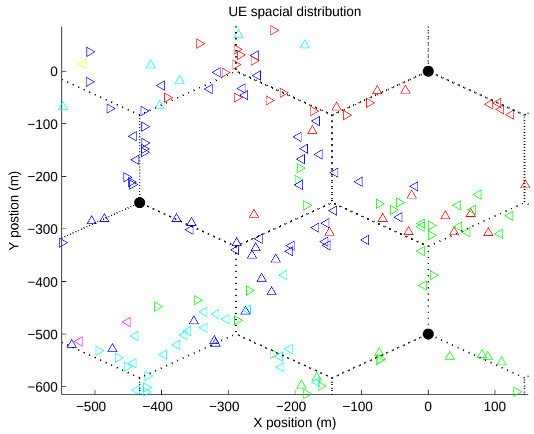

Figure 13: UE position map - Geometry ≈ -2.5dB

5.2.2 Interference profile for heterogeneous scenario

The heterogeneous network, or HetNet, scenario considered in this thesis is divided in two sub-cases, HetNet Configuration 1, and HetNet Configuration 4b as previously shown on Table 2. DIP profiles for both configurations and two values of hard handover margin are analyzed following the same principles as in Section 5.2.1.The unconditional and conditional DIP profiles for both configurations are depicted in Figure 14. In the figure's legend, c1 denotes HetNet Configuration 1 and c4b denotes HetNet Configuration 4b. HO: 0dB denotes 0 dB hard handover margin, or ideal cell selection and HO: 3dB denotes 3 dB hard handover margin. The horizontal axis represents geometry positions, except for the last element "All" which represents the unconditional DIP profile. Note that only two strongest conditional DIP profiles are depicted for each simulated case.

From Figure 14 it is clearly observed that at lower geometries the strongest conditional DIP for HetNet cases with 3 dB hard handover margin is dominant. Also, all strongest unconditional and conditional DIP are much dominant that the second strongest. These observations support the belief that in many LTE deployment scenarios exists a dominant source of interference.

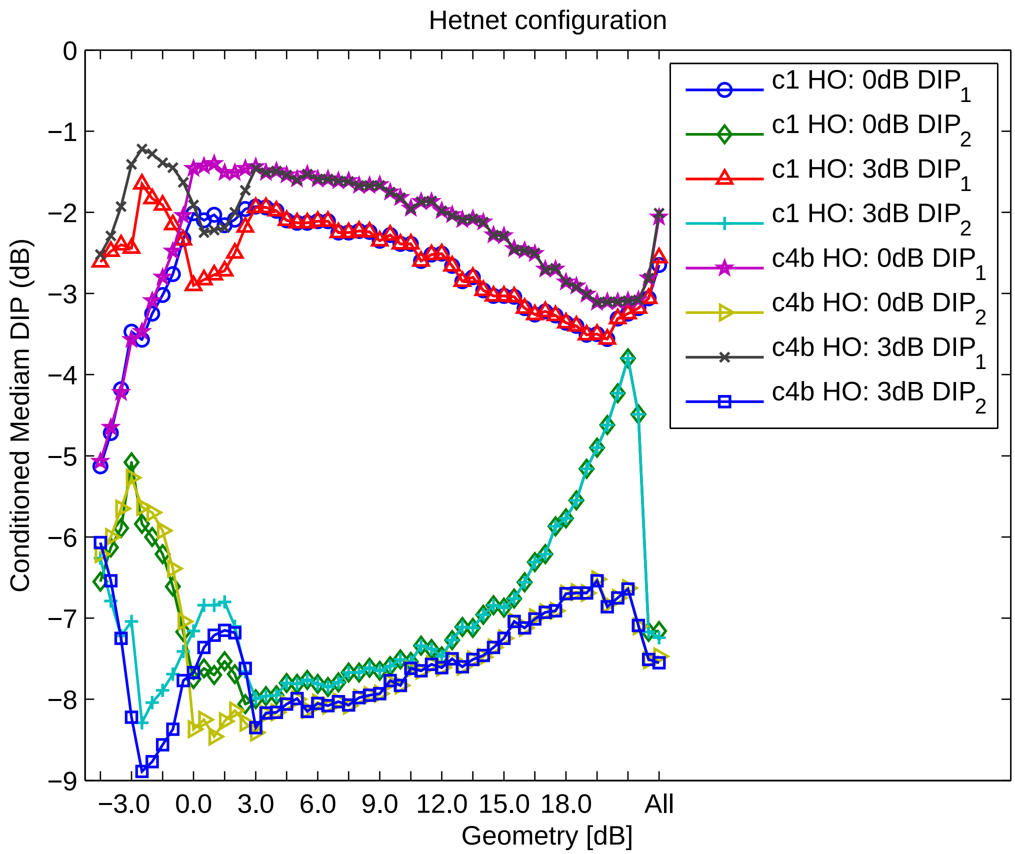

Figure 14: DIP profile [dB] for HetNet Configuration 1 and 4b

6 Simulation results

The advanced linear interference aware receivers were modeled in Chapter 3 using mathematical tools developed in random matrix theory. Specifically, the emulation using the Wishart distribution of two IRC interference covariance matrix estimation algorithms was presented. These models of advanced receivers were applied in an LTE-Advanced system level simulator in order to evaluate the performance of advanced interference aware receivers.

This chapter summarizes the numerical performance of the different linear receiver algorithms studied in the deployment scenarios of interest. The methodology utilized to summarize the results is inspired from inferential statistics, and it has not been used in the reviewed telecommunications literature. In a nutshell, the used statistical methods have been motivated by the need to draw more generic conclusions about the performance of linear receivers from a large amount of results generated by system level simulations. The obtained statistical summary provides a wider comparative insight of how different linear receiver algorithms perform across different deployment scenarios. This contrasts with a per-scenario summary where only a single set of results per scenario are analyzed together as it is normally done in the literature [24]. An example of a scenario summary can be found in Annex B.

A total of 70 scenarios were studied during the research period. These include five network topologies, a set of antenna configurations and two values of hard handover margin as it is explained in Section 6.1.

Figure 15 depicts the studied combination of network topologies and antenna configurations. A set of performance indicators and spectral efficiency summaries were obtained for each studied scenario. These indicators are useful when comparing directly few number of specific scenarios (see for example [24]), but for the specific case of this thesis, presenting all the information only distracts the attention of the reader from the objectives of the study. For interested readers, a detailed example of these performance indicators is presented in Annex B.

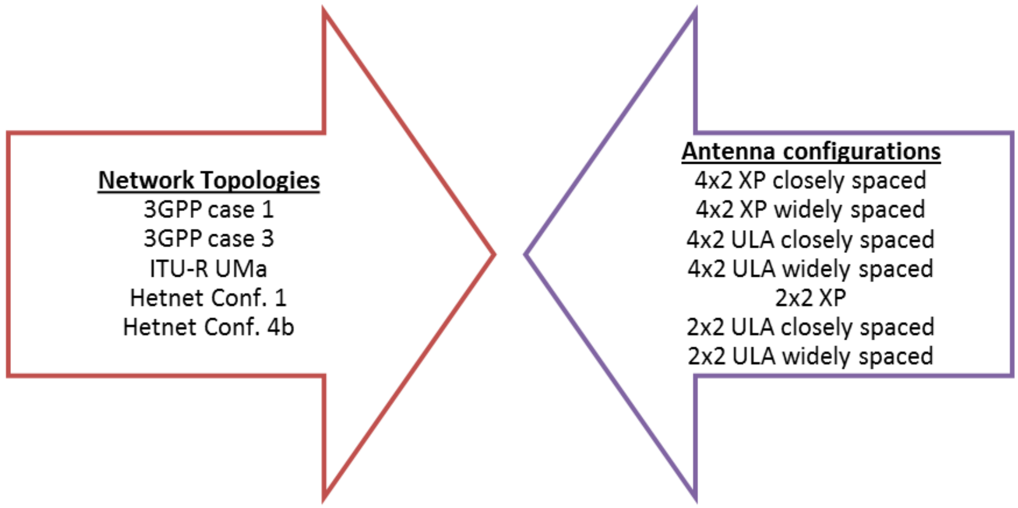

Figure 15: Simulated scenarios

6.1 Scenarios of interest

The scenarios of interest cover homogeneous and heterogeneous networks (Section 4.1) with different antenna configurations (Section 4.4) and two different values of hard-handover margin. In total 35 different network deployments, summarized in Figure 15, are studied. This number is obtained by the combination of five network topologies with the considered antenna configurations. The 2×2 LTE-Advanced system can have ULA or XP antenna configurations at the eNB. Furthermore, the 2×2 ULA antenna configuration can be closely spaced or widely spaced as explained in Section 4.4. Thus, three antenna configurations are available for the 2×2 case. Similarly, the 4×2 LTE-Advanced system can have ULA or XP antenna configurations at the eNB. In a 4×2 configuration both ULA and XP can be closely spaced or widely spaced. Thus, four antenna configurations are available for the 4×2 case. In total there are 7 possible antenna configurations and the total number of network deployment combinations is $5 \times 7 = 35$. Finally, two hand-over margins are considered. Thus, the total number of scenarios of interest is 70. Table 9 summarizes the simulation scenarios and provides reference to the simulation assumptions. The performance of the linear receivers is studied in each scenario of interest.

Table 9: Scenarios of interest

Network topology	Simulation assumptions
3GPP Case 1	See tables 3, 2 and 10
3GPP Case 3	See tables 3, 2 and 10
ITU-R UMa	See tables 4, 2 and 10
HetNet Configuration 1	See tables 4, 2 and 10
HetNet Configuration 4b	See tables 4, 2 and 10

6.2 Simulation assumptions

The main simulation assumptions are kept similar across all scenarios of interest. Each linear receiver is analyzed assuming the XP and ULA antenna configurations as explained in the previous section. In addition, the UE has a cross-polarized antenna configuration as described in Table 10.

6.3 Summary of methodology

It is common to use statistical methods in order to make conclusions from large data sets. In this particular case, the data set represents the obtained mean Spectral Efficiency (SE) and cell-edge spectral efficiency achieved by the considered linear receivers in the simulated scenarios of interest. The assumptions for the statistical analysis are the following. It is assumed that the space Ω exists where all possible configurations for the LTE-Advanced performance studies are included. Also, a subset of the space Ω is defined as $\Xi \subset \Omega$. In this study, Ξ is composed by all the scenarios of interest described in sub-section 6.1. That is, $\Xi = \{\xi_1, \cdots, \xi_{70}\}$. Furthermore, all considered linear receivers in this thesis (Chapter 3) are studied in each scenario of interest.

Two performance indicators are selected as observed samples for each scenario of interest, $\xi_j \in \Xi$. These performance indicators are the mean spectral efficiency per sector (mean SE/sector) denoted as m_j and cell-edge spectral efficiency per sector per UE (5%-cdf SE/Sector/UE) denoted as c_j. The observed samples (m_j and c_j) are considered to be random variables coming from the unknown CDF distributions $\mathrm{F}_{\mathrm{mean}}$ and $\mathrm{F}_{\mathrm{CellEdge}}$. These distributions summarize the achievable mean spectral efficiency and cell-edge spectral efficiency in the subset Ξ.

Using the random samples m_j and c_j, the empirical-CDFs $\mathrm{F}'_{\mathrm{mean}}$ and $\mathrm{F}'_{\mathrm{CellEdge}}$ along with their average values and standard deviations are computed per receiver algorithm. The obtained results are presented in Section 6.4. The mean SE empirical CDF and cell-edge SE empirical CDF are depicted in Figure 16 and Figure 17 respectively. These figures provide performance comparisons for linear receiver algorithms across all scenarios of interested.

6.4 Comparison of results

The comparison between linear receivers across the scenarios of interest is done by observing the spectral efficiency empirical CDFs, the average values and standard deviations. The average values and standard deviations of the spectral efficiency observations per linear receiver algorithm are shown in Table 11 and Table 12 for mean SE and cell-edge SE respectively. These statistical descriptions provide an insight on the general performance of linear interference aware receivers in the LTE-Advanced system.

Table 11: Average and standard deviation of mean SE (bps/Hz/sector)

Linear receiver	Average	Standard deviation
MRC	2.3527	0.9021
MRC_{PA}	2.4525	0.9821
LMMSE_{CL}	2.6728	1.0388
$\text{LMMSE-IRC}_{\text{WI-DATA}}$	2.3468	1.0144
$\text{LMMSE-IRC}_{\text{WI-RS}}$	2.7653	1.0799
IRC	2.8010	1.0804

Table 12: Average and standard deviation of cell-edge SE (bps/Hz/UE/sector)

Linear receiver	Average	Standard deviation
MRC	0.0498	0.0159
MRC_{PA}	0.0525	0.0167
LMMSE_{CL}	0.0529	0.0171
$\text{LMMSE-IRC}_{\text{WI-DATA}}$	0.0511	0.0186
$\text{LMMSE-IRC}_{\text{WI-RS}}$	0.0585	0.0212
IRC	0.0620	0.0219

The analysis of results have the following structure. First, the results for the MRC, MRC_{PA} and LMMSE_{CL} receivers are analyzed together because these are well-know receivers that are continuously used in 3GPP investigations [46]. Second, the results for the linear interference aware receivers $\text{LMMSE-IRC}_{\text{WI-DATA}}$, $\text{LMMSE-IRC}_{\text{WI-RS}}$ and IRC are analyzed. Finally, the results for the LMMSE_{CL}, $\text{LMMSE-IRC}_{\text{WI-RS}}$ and IRC are analyzed together.

Tables 11 and 12 show clear performance differences between the MRC, MRC_{PA} and LMMSE_{CL} receivers in mean sector SE and cell-edge SE. The white-noise MRC receiver performs poorly in average compared with the MRC_{PA} and LMMSE_{CL} receivers. The MRC_{PA} performs 4.2% better in mean SE and 5.4% better in cell-edge SE than the MRC. The LMMSE_{CL} performs 13.6% better in mean SE and 6.2% better in cell-edge SE than the MRC. However, it is observed that standard deviation of the MRC is the smallest meaning that its performance across the studied scenarios varies less than other algorithms.

By looking also at the CDFs curves from Figures 16 and 17, it is observed that the LMMSE_{CL} performs clearly better in the mean SE sense and very similarly in the cell-edge SE sense compared with the MRC_{PA}. The superior performance of the LMMSE_{CL} in mean sector spectral efficiency over the other MRC algorithms can be explained due to the use of rank 2 transmissions in the system. The LMMSE_{CL} can suppress the intra-site co-layer interference generated by the rank 2 usage because it possesses the knowledge of the interfering co-layer channel coefficients. Co-layer interference suppression is not performed by the MRC nor by the MRC_{PA}. However, rank 2 usage is not expected in cell-edge UEs due to the low SINR and consequently

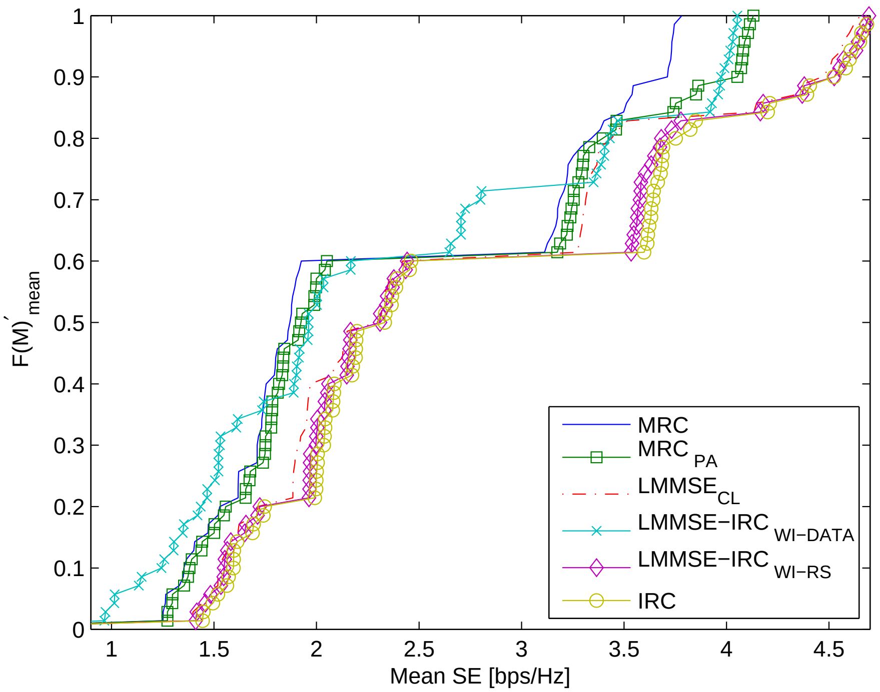

Figure 16: Empirical mean SE CDF

degradation of the channel estimates. Thus, at cell-edge the performance between the $\mathrm{MRC_{PA}}$ and $\mathrm{LMMSE_{CL}}$ is similar across the scenarios of interest.

The performance results for the interference aware receivers $\mathrm{LMMSE\text{-}IRC_{WI\text{-}DATA}}$ and $\mathrm{LMMSE\text{-}IRC_{WI\text{-}RS}}$ have to be analyzed considering the performance upper-limit set by the IRC receiver as previously discussed in Section 3.1. The first obvious observation from Table 11, Table 12, Figure 16 and Figure 17 is that the performance of the data-based interference aware receiver ($\mathrm{LMMSE\text{-}IRC_{WI\text{-}DATA}}$) is very poor compared with the performance of the reference-symbol-based interference aware receiver ($\mathrm{LMMSE\text{-}IRC_{WI\text{-}RS}}$). Also, the standard deviation for the $\mathrm{LMMSE\text{-}IRC_{WI\text{-}DATA}}$ results are very small. These observations tell us that the $\mathrm{LMMSE\text{-}IRC_{WI\text{-}DATA}}$ achieved spectral efficiency values are constantly small across all scenarios.

The explanation why $\mathrm{LMMSE\text{-}IRC_{WI\text{-}RS}}$ has better performance than $\mathrm{LMMSE\text{-}IRC_{WI\text{-}DATA}}$ is the IRC interference covariance estimation algorithm. The $\mathrm{LMMSE\text{-}IRC_{WI\text{-}RS}}$ covariance has two clear defined elements: The intra-site interference covariance estimated directly from reference signals and the inter-site covariance matrix estimated from the residual information from the reference signals. The $\mathrm{LMMSE\text{-}IRC_{WI\text{-}DATA}}$ covariance has one element which is estimated using data samples. The estimation procedure based on reference signals is the reason why the reference-symbol-based interference aware receiver has a better performance compared with the data-sample based interference aware receiver.

Comparing the worse performing receivers in mean SE, it is observed that the

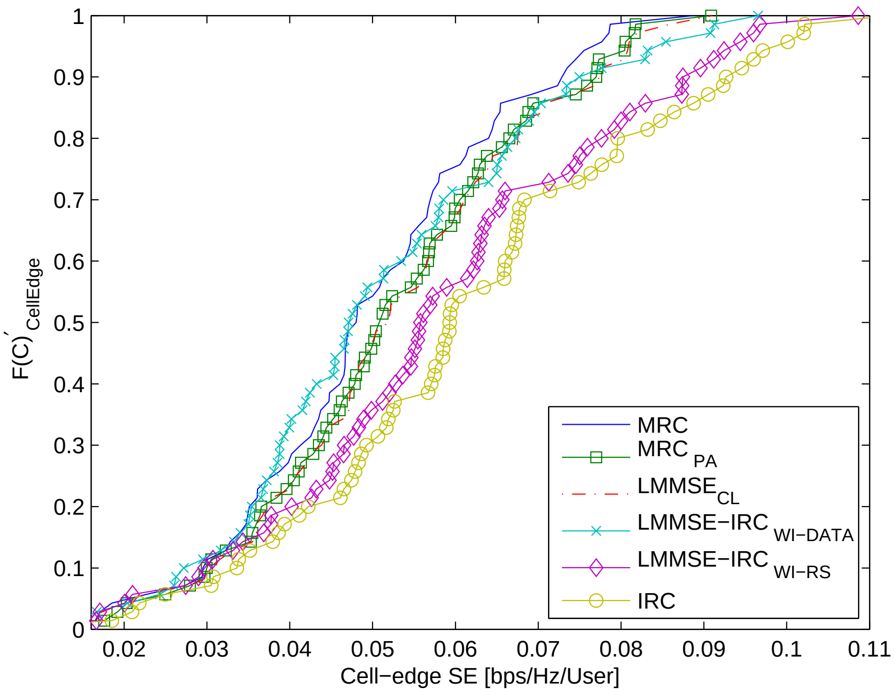

Figure 17: Empirical cell-edge SE CDF

MRC receiver performs better in mean SE than the LMMSE-IRC$_{\text{WI-DATA}}$ receiver. In cell-edge SE the LMMSE-IRC$_{\text{WI-DATA}}$ receiver performs slightly better than the MRC but worse than the MRC$_{\text{PA}}$. This can be explained by remembering that the data-based interference aware receiver estimates its interference covariance utilizing the all received data samples on the PDSCH. The LMMSE-IRC$_{\text{WI-DATA}}$ covariance matrix estimation algorithm does not take fully advantage of the less-interfered RS pilots to perform channel estimation and thus there is a considerable performance degradation.

In addition, it is observed that the LMMSE-IRC$_{\text{WI-RS}}$ receiver achieves 98.7% of the IRC performance in mean SE and 94.3% of the performance in cell-edge SE in average across the scenarios of interest. This result shows that the Wishart-based model of the reference-symbol-based advanced receiver works well in all tested scenarios. Furthermore, in every point of the CDFs, the IRC receiver achieves the best performance as expected.

The comparison between baseline linear receivers with advanced interference aware linear receivers is done by comparing the best performing of both groups. The best performing baseline linear receiver is the LMMSE$_{\text{CL}}$ and the best performing advanced interferer aware linear receiver is the LMMSE-IRC$_{\text{WI-RS}}$ (the performance of the IRC is considered the upper-limit of achievable performance). The LMMSE-IRC$_{\text{WI-RS}}$ performs slightly better in mean SE than the LMMSE$_{\text{CL}}$ achieving a gain of 3.5% in mean SE. However, in the cell-edge SE sense the LMMSE-IRC$_{\text{WI-RS}}$ achieves a gain of 10.6% against the LMMSE$_{\text{CL}}$ across the scenarios of interest as can be seen from Figure 17 and Table 12. The better cell-edge performance of the LMMSE-IRC$_{\text{WI-RS}}$ is due to the inter-site interference suppression capabilities of the interfere aware linear receiver. In Chapter 5 Section 5.2, it was shown that a dominant source of interference exists at cell-edge. It is worth repeating that these average gains are a generalization across multiple scenarios. There are specific scenarios where the gains of LMMSE-IRC$_{\text{WI-RS}}$ receiver are much higher compared with the LMMSE$_{\text{CL}}$ [24].

Table 10: Simulation assumptions

Parameter	**Value**
Simulation time	3.0 s
Number of simulation runs	30 runs
Traffic model	Full buffer
Simulation scenario	See Table 9
eNB antenna configuration	2 antenna elements ULA 0.5 λ spacing - 45°degrees slant ULA 4.0 λ spacing - 45°degrees slant XP - 0°/ 90°degrees slant 4 antenna elements ULA 0.5 λ spacing - 45°degrees slant ULA 4.0 λ spacing - 45°degrees slant XP - 0°/ 90°degrees slant, 0.5 λ spacing XP - 0°/ 90°degrees slant, 4.0 λ spacing
UE antenna configuration	2 antenna elements, XP 0°degrees slant
MIMO scheme	2×2 SU-MIMO with dynamic rank adaptation (TM4) 4x2 SU-MIMO with dynamic rank adaptation (TM9)
Number of UE per sector	3GPP Case 1, 3GPP Case 3 and ITU-R UMa : 10 UEs Heterogeneous network Configuration 1 : 25 UEs Heterogeneous network Configuration 4b : 30 UEs See Table 2
Codebook	Rel´8 TX codebook
TD-FD scheduler	Proportional Fair - Proportional fair
Number of samples for Wishart distribution	$N_{\mathrm{CRS}} = 12$ $N_{\mathrm{DMRS}} = 12$ $N_{\mathrm{DS}} = 120$
Inter-cell interference model	Transmission with random rank and PMI in interfering cells
Channel estimation for demodulation	Realistic (via AVI tables)
Channel estimation for CSI	2×2 case: CRS based 4×2 case: CSI-RS based
Reference symbol overhead	2Tx Rel´8 CRS (legacy) DMRS 12 RE/PRB CSI-RS overhead 4 RE/PRB
Cell selection	RSRP
Hard handover margin	0 dB , 3 dB

7 Conclusions and future work

The modeling of advanced linear interference aware receivers, which are possible implementations of the IRC receiver, was performed using random matrix theory. To build the correspondent models for advanced linear receivers, two IRC interference covariance matrix estimation algorithms have been emulated using the Wishart distribution. This emulation process allows the modeling of advanced linear interference aware receivers without the need of baseband signals.

The evaluation of advanced linear interference aware receivers was performed with an LTE-Advanced system level simulator in which the already mentioned modeling of advanced linear receivers has been applied. Two advanced interference aware receivers were studied, the first based on data samples to estimate the IRC interference covariance matrix and the second based on reference symbols. Also, the IRC and other commonly used 3GPP baseline linear receivers (MRC, $\mathrm{MRC_{PA}}$ and $\mathrm{LMMSE_{CL}}$) have been used for comparisons. To get a wider insight on the potential performance improvement, system simulations were performed for a large number of deployment scenarios of interest and the results have been summarized using statistical methods as seen in Section 6.3 and Section 6.4

In the first part of the section, conclusions of the study are presented. This is followed by possible topics for future research.

7.1 Conclusions

The first conclusion from this study is that in many LTE-deployment scenarios exists many sources of interference which can be detected. In particular, dominant interferer exists which contributes to nearly 50% of the total interference power as shown in Chapter 5. This dominant interferer can be mitigated with the IRC receiver. It was also shown that it is possible to apply random matrix theory in order to model practical IRC implementations without the need of baseband signals.

From the obtained CDFs and summaries of system performance, a general observation is that the interference rejection combiner outperforms the best-performing 3GPP baseline linear receiver $\mathrm{LMMSE_{CL}}$ in both mean spectral efficiency and cell-edge spectral efficiency as expected. This means that practical IRC implementations could provide performance improvements in LTE-Advanced. It is observed that the reference-symbol-based advanced linear receiver achieves the closest performance to the IRC whereas the data-sample-based advanced linear receiver has a poor performance compared with the MRC receiver. The good performance of the $\mathrm{LMMSE\text{-}IRC_{WI\text{-}RS}}$ receiver can be explained by the IRC interference covariance estimation algorithm employed. The $\mathrm{LMMSE\text{-}IRC_{WI\text{-}RS}}$ covariance matrix is composed by two parts: the intra-site interference covariance matrix estimated directly from reference symbols and the inter-site covariance matrix estimated from the residual information from reference symbols. The $\mathrm{LMMSE\text{-}IRC_{WI\text{-}DATA}}$ covariance matrix has a single element which includes the intra-site and inter-site interference information and is estimated using data samples. The covariance estimation procedure based on reference symbols is the reason why the reference-symbol-based interference aware receiver has a notoriously better performance compared with the data-sample based interference aware receiver.

From the mean spectral efficiency perspective, it is observed that the baseline linear LMMSE_{CL} receiver has relatively similar performance compared with the advanced linear $\text{LMMSE-IRC}_{\text{WI-RS}}$ receiver in most points of the CDF curve depicted in Figure 16. It is also observed that the performance gap between $\text{LMMSE-IRC}_{\text{WI-RS}}$ and IRC is very small. It is concluded that linear advanced receivers bring small performance improvement to the sector mean spectral efficiency compared with the existing best-performing baseline receiver.

From the cell-edge spectral efficiency perspective, it is clearly observed that there is a performance improvement given by the advanced $\text{LMMSE-IRC}_{\text{WI-RS}}$ receiver compared with the LMMSE_{CL} receiver. It is also observed that the performance gap between $\text{LMMSE-IRC}_{\text{WI-RS}}$ and IRC is larger than for the mean spectral efficiency case. This is due to the fact that channel estimation is less accurate at cell-edge. It is concluded that linear advanced receivers improve the performance of cell-edge UE compared with the existing best-performing baseline receiver.

Furthermore, as the conclusions are taking into account many LTE-Advanced homogeneous and heterogeneous deployment scenarios. The results can be extrapolated for any dense LTE-Advanced deployment.

7.2 Future work

The focus of this study has been primarily user equipment linear receivers. Future work on user equipment receivers could concentrate on modeling and analyzing the performance of non-linear receivers compared with linear advanced receivers. This includes the signaling and trade-off between signaling overhead and capacity improvement. For example, a potential non-linear receiver to be study is the successive interference rejection receiver.

Also, the performance was studied using single-user MIMO transmission. It would be interesting to investigate what is the impact of advanced linear receivers and non-linear receivers combined with other LTE-Advanced interference coordination mechanism such as CoMP and eICIC.

In addition, the opposite of what has been done in this thesis can also be investigated. Instead of emulating the IRC interference covariance matrix estimation algorithm in order to evaluate the advanced receivers performance without explicit need for baseband signals, a proper modeling of interference environment applicable to link level simulators can be investigated

Furthermore, in this thesis receiver enhancements are completely compatible with current LTE-Advanced specifications. Future work can focus on investigate network coordination schemes that will aid linear advanced receivers to perform better interference rejection.

References

[1] Ericsson, "Traffic and Market Data Report," Nov 2011, Available at: http://www.ericsson.com/news, Accessed in 2.2.2012.

[2] Cisco, "Cisco Visual Networking Index: Global Mobile Data Traffic Forecast Update, 2010 - 2015," Feb 2011, Available at: http://www.cisco.com/, Accessed in 2.2.2012.

[3] ITU, "ITU paves way for next-generation 4G mobile technologies," press release, ITU, Oct. 2008.

[4] J. Winters, "Optimum Combining in Digital Mobile Radio with Cochannel Interference," in *IEEE Journal on Selected Areas in Communications*, July 1984, vol. 2, pp. 528 –539.

[5] M. Chiani, M. Win, A. Zanella, R. Mallik, and J. Winters, "Bounds and approximations for optimum combining of signals in the presence of multiple cochannel interferers and thermal noise," in *IEEE Transactions on Communications*, Feb 2003, vol. 51, pp. 296 – 307.

[6] C.-H. Yu and O. Tirkkonen, "Characterization of SINR uncertainty due to spatial interference variation," in *IEEE International Workshop on Signal Processing Advances in Wireless Communications*, June 2010, pp. 1–5.

[7] G. Klang, *On Interference Rejection in Wireless Multichannel Systems, D.Sc. Dissertation*, Royal Institute of Technology, Stockholm, Sweden, 2003.

[8] J. Karlsson and J. Heinegard, "Interference rejection combining for GSM," in *IEEE International Conference on Universal Personal Communications*, Sept 1996, vol. 1, pp. 433 –437.

[9] D. Bladsjo, A. Furuskar, S. Javerbring, and E. Larsson, "Interference cancellation using antenna diversity for EDGE-enhanced data rates in GSM and TDMA/136," in *IEEE Vehicular Technology Conference*, 1999, vol. 4, pp. 1956 –1960.

[10] A. Kuzminskiy, C. Luschi, and P. Strauch, "Comparison of linear and MLSE spatio-temporal interference rejection combining with an antenna array in a GSM system," in *IEEE Vehicular Technology Conference Proceedings*, 2000, vol. 1, pp. 172 –176.

[11] S. Craig and J. Axnas, "A system performance evaluation of 2-branch interference rejection combining," in *IEEE Vehicular Technology Conference*, 2002, vol. 3, pp. 1887 – 1891.

[12] K. Kim and G. Stuber, "Interference cancelling receiver for range extended reception in TDMA cellular systems," in *IEEE Vehicular Technology Conference*, Oct. 2003, vol. 2, pp. 1030 – 1034.

[13] A. Mostafa, R. Kobylinski, I. Kostanic, and M. Austin, "Single antenna interference cancellation (SAIC) for GSM networks," in *IEEE Vehicular Technology Conference*, Oct. 2003, vol. 2, pp. 1089–1093.

[14] A. Mostafa, "Single antenna interference cancellation (SAIC) method in GSM network," in *IEEE Vehicular Technology Conference*, Sept. 2004, vol. 5, pp. 3748–3752.

[15] R. Meyer, W. Gerstacker, R. Schober, and J. Huber, "A single antenna interference cancellation algorithm for GSM," in *IEEE Vehicular Technology Conference*, May 2005, vol. 2, pp. 821–825.

[16] M. Pukkila, G. Mattellini, and P. Ranta, "Constant modulus single antenna interference cancellation for GSM," in *IEEE Vehicular Technology Conference*, May 2004, vol. 1, pp. 584 – 588.

[17] D. Astely and A. Artamo, "Uplink spatio-temporal interference rejection combining for WCDMA ," in *IEEE Workshop on Signal Processing Advances in-Wireless Communications*, 2001, pp. 326 –329.

[18] H. Schotten and J. Rossler, "System performance gain by interference cancellation in WCDMA dedicated and high-speed downlink channels," in *IEEE Vehicular Technology Conference*, 2002, vol. 1, pp. 316–320.

[19] J. Dumont, S. Lasaulce, and J.-M. Chaufray, "On the choice of the best linear multi-antenna receiver to combat downlink adjacent channel interference in WCDMA networks," in *IEEE Vehicular Technology Conference*, Sept. 2004, vol. 3, pp. 2168–2172.

[20] T. Nihtila, J. Kurjenniemi, and M. Lampinen, "Effect of Ideal Inter-Cell Interference Cancellation to HSDPA System Performance," in *IEEE International Symposium on Personal, Indoor and Mobile Radio Communications*, Sept. 2007, pp. 1 –5.

[21] L. Thiele, M. Schellmann, T. Wirth, and V. Jungnickel, "On the value of synchronous downlink MIMO-OFDMA systems with linear equalizers," in *IEEE International Symposium onWireless Communication Systems*, Oct. 2008, pp. 428 –432.

[22] Y. Ohwatari, N. Miki, T. Asai, T. Abe, and H. Taoka, "Performance of Advanced Receiver Employing Interference Rejection Combining to Suppress Inter-Cell Interference in LTE-Advanced Downlink," in *IEEE Vehicular Technology Conference*, Sept. 2011, pp. 1–7.

[23] M. Lampinen, F. Del Carpio, T. Kuosmanen, T. Koivisto, and M. Enescu, "System-level Modeling and Evaluation of Interference Suppression Receivers in LTE System," in *IEEE Vehicular Technology Conference*, May 2012, pp. 1–5.

[24] K. Pietikäinen, F. Del Carpio, M. Lampinen, T. Koivisto, H.-L. Maattanen, and M. Enescu, "System-level performance of interference suppression receivers in LTE system," in *IEEE Vehicular Technology Conference*, May 2012, pp. 1–5.

[25] H. Li and H. V. Poor, "Impact of Channel Estimation Errors on Multiuser Detection via the Replica Method," in *EURASIP Journal on Wireless Communications and Networking*, 2005, vol. 2005, pp. 175–186.

[26] H. Holma and A. Toskala, *WCDMA for UMTS: Radio Access for Third Generation Mobile Communications*, John Wiley and Sons, Chichester, West Sussex, England, 2004.

[27] A. Riikonen, *Mobile Internet usage - network traffic measurements, Master's thesis*, Helsinki University of Technology, Department of Communications and Networking, Espoo, Finland, 2009.

[28] M. Rinne and O. Tirkkonen, "LTE, the radio technology path towards 4G," in *Comput. Commun.*, Oct. 2010, vol. 33, pp. 1894–1906.

[29] 3GPP, "Evolved Universal Terrestrial Radio Access (E-UTRA); Long Term Evolution (LTE) physical layer; General description," TS 36.201, 3rd Generation Partnership Project (3GPP), Dec. 2007.

[30] 3GPP, "Evolved Universal Terrestrial Radio Access (E-UTRA); LTE physical layer; General description," TS 36.201, 3rd Generation Partnership Project (3GPP), Dec. 2010.

[31] ITU, "Requirements related to technical performance for IMT-Advanced radio interface(s)," ITU-R M.2134, ITU, 2008.

[32] 3GPP, "Requirements for Evolved UTRA (E-UTRA) and Evolved UTRAN (E-UTRAN)," TR 25.913, 3rd Generation Partnership Project (3GPP), June 2005.

[33] E. Dahlman, S. Parkvall, J. Sköd, and P.Berming, *3G evolution: HSPA and LTE for Mobile Broadband*, Academic Press, Oxford, UK, 2008.

[34] H. Holma and A. Toskala, *LTE for UMTS: OFDMA and SC-FDMA Based Radio Access*, John Wiley and Sons, Chichester, West Sussex, England, 2009.

[35] P. Lescuyer and T. Lucidarme, *Evolved Packet System (EPS): The LTE and SAE evolution of 3G UMTS*, John Wiley and Sons, Chichester, West Sussex, England, 2008.

[36] M. Rinne, *Convergence of packet communications over the evolved mobile networks, signal processing and protocol performance, D.Sc. Dissertation*, Aalto University, Espoo, Finland, 2008.

[37] A. Larmo, M. Lindström, M. Meyer, G. Pelletier, J. Torsner, and H. Wiemann, "The LTE link-layer design," in *IEEE Communications Magazine*, April 2009, pp. 52–59.

[38] 3GPP, "Evolved Universal Terrestrial Radio Access (E-UTRA); Physical channels and modulation," TS 36.211, 3rd Generation Partnership Project (3GPP), Mar. 2011.

[39] Motorola, "Technical White Paper, Long Term Evolution (LTE)," 2007, Available at: http://www.motorola.com/, Accessed in 3.2.2012.

[40] Y.-H. Nam, Y. Akimoto, Y. Kim, M. il Lee, K. Bhattad, and A. Ekpenyong, "Evolution of reference signals for LTE-advanced systems," in *IEEE Communications Magazine*, February 2012, vol. 50, pp. 132 –138.

[41] K. Takeda, Y. Kishiyama, M. Tanno, and T. Nakamura, "Investigation of Two-Dimensional Orthogonal Sequence Mapping to Multi-Layer Reference Signal for LTE-Advanced Downlink," in *IEEE Vehicular Technology Conference*, Sept 2010, pp. 1-5.

[42] 3GPP, "REV-090003r1, IMT-Advanced Evaluation Workshop," Dec. 2009.

[43] H.-L. Määttänen, *Linear trasnmission methods and feedback for downlink MIMO systems, D.Sc. Dissertation*, Aalto University publication series, Espoo, Finland, 2012.

[44] A. Hottinen, R. Wichman, and O. Tirkkonen, *Multi-Antenna Transceiver Techniques for 3g and Beyond*, John Wiley and Sons, Chichester, West Sussex, England, 2003.

[45] N. Jindal, "MIMO Broadcast Channels With Finite-Rate Feedback," in *IEEE Transactions on Information Theory*, Nov. 2006, vol. 52, pp. 5045 –5060.

[46] LG Electronics, Motorola Mobility, Intel, Marvell, Samsung, ETRI, Orange, Renesas and Huawei, "Proposal for UE receiver assumption in CoMP simulations," Tdoc R1-110586, 3rd Generation Partnership Project (3GPP), Jan. 2011.

[47] Renesas Mobile Europe Ltd., "Interference aware receiver modeling at system level," Tdoc R1-112311, 3rd Generation Partnership Project (3GPP), Aug. 2011.

[48] Nokia, Nokia Siemens Networks, "On advanced UE MMSE receiver modelling in system simulations," Tdoc R1-111031, 3rd Generation Partnership Project (3GPP), Feb. 2011.

[49] S. M. Kay, *Fundamentals of statistical signal processing: estimation theory*, Prentice-Hall, New Jersey, USA, 1993.

[50] R. Muirhead, *Aspects of Multivariate Statistical Theory*, John Wiley and Sons, New York, USA, 1982.

[51] N. Madras, *Lectures on Monte Carlo Methods*, Fields Institute Monographs. American Mathematical Society, Rhode Island, USA, 2002.

[52] H. Wang and E. Tuomaala, "Effective SINR Approach of Link to System Mapping in OFDM/Multi-Carrier Mobile Network," in *The 2nd IEE International Conference on Mobile Technology, Applications and Systems*, Nov. 2015.

[53] I. Kovacs, M. Kuusela, E. Virtej, and K. Pedersen, "Performance of MIMO Aware RRM in Downlink OFDMA," in *IEEE Vehicular Technology Conference*, May 2008, pp. 1171 –1175.

[54] 3GPP, "Physical layer aspects for evolved universal terrestrial radio access (Release 9)," TR 36.814, 3rd Generation Partnership Project (3GPP), Mar. 2010.

[55] 3GPP, "Spacial channel model for Multiple Input Multiple Output (MIMO) simulations," TR 25.996, 3rd Generation Partnership Project (3GPP), June 2007.

[56] ITU-R, "Guidelines for evaluation of radio interface technologies for IMT-Advanced," TR M.2135, International Telecommunication Union (ITU), Nov. 2008.

[57] S. Strzyz, K. Pedersen, J. Lachowski, and F. Frederiksen, "Performance optimization of pico node deployment in LTE macro cells," in *Future Network Mobile Summit (FutureNetw)*, June 2011, pp. 1–9.

[58] Renesas Mobile Europe Ltd., "On DIP profiles conditioned to -3dB geometry," Tdoc R4-120525, 3rd Generation Partnership Project (3GPP), Feb. 2012.

[59] Nokia, Nokia Siemens Networks, "On DIP distribution for Advanced Receivers Studies," Tdoc R4-120311, 3rd Generation Partnership Project (3GPP), Feb. 2012.

[60] Timm and H. Neil, *Applied Multivariate Analysis*, Springer, New York, USA, 2002.

[61] A. M. Tulino and S. Verdú, *Random Matrix Theory and Wireless Communications*, Now publishers, Delft, The Netherlands, 2004.

[62] M. S. Srivastava, "On the Complex Wishart Distribution," in *The Annals of Mathematical Statistics*, 1965, vol. 36, pp. 313–315.

A Introduction to random matrix theory

A.1 Multivariate normal distribution

A.1.1 Moments of random vector

Let $\mathbf{X}$ be a random $m \times 1$ vector $\mathbf{X} = (X_1, \ldots, X_m)'$, the mean or expectation of $\boldsymbol{X}$ is $\mathrm{E}(\boldsymbol{X})$ is defined to be a vector of expectations

$$\mathrm{E}(\mathbf{X}) = \begin{pmatrix} E(X_1) \\ \vdots \\ E(X_m) \end{pmatrix}. \tag{A.1}$$

If $\boldsymbol{X}$ has mean μ the covariance matrix of $\boldsymbol{X}$ is defined to be the $m \times m$ matrix

$$\boldsymbol{\Sigma} = \mathrm{Cov}(\mathbf{X}) = \mathrm{E}\left[(\mathbf{X} - \mu)(\mathbf{X} - \mu)'\right]. \tag{A.2}$$

The $i - j$ th element of $\boldsymbol{\Sigma}$ is

$$\sigma_{ij} = \mathrm{E}\left[(X_i - \mu_i)(X_j - \mu_j)'\right],$$

the covariance between the X_i and X_j, and the $i - i$ th element is

$$\sigma_{ij} = \mathrm{E}\left[(X_i - \mu_i)^2\right],$$

the variance of X_i, so the diagonal elements of Σ must be non-negative. Also, Σ is symmetric, $\Sigma = \Sigma'$. A symmetric matrix $\boldsymbol{A}$ is called non-negative definite if $\alpha' \boldsymbol{A} \alpha \geq 0$ for all $\alpha \in \mathrm{R}^{\mathrm{n}}$. We can say the matrix Σ is covariance matrix if and only if it is non-negative definite [50].

A.1.2 Useful properties

Let us suppose the $m \times m$ matrix $\boldsymbol{\Sigma}_y$ is the covariance matrix of the random $m \times 1$ vector $\boldsymbol{Y}$, the expectation is $\mathrm{E}(\boldsymbol{Y}) = 0$. If we define a scaled random vector $\boldsymbol{X} = \mathbf{C}\boldsymbol{Y}$, where $\mathbf{C}$ has dimensions $m \times m$ and $\mathbf{C}'$ exits. The mean of $\boldsymbol{X}$ is zero and the covariance matrix is

$$\begin{aligned} \mathrm{Cov}(\boldsymbol{X}) &= \mathrm{Cov}(\mathbf{C}\boldsymbol{Y}) \\ &= \mathrm{E}[\mathbf{C}\boldsymbol{Y}\boldsymbol{Y}^{\mathrm{H}}\mathbf{C}^{\mathrm{H}}] \\ &= \mathbf{C}\mathrm{E}[\boldsymbol{Y}\boldsymbol{Y}^{\mathrm{H}}]\mathbf{C}^{\mathrm{H}} \\ &= \mathbf{C}\Sigma_{\mathrm{y}}\mathbf{C}^{\mathrm{H}} \end{aligned} \tag{A.3}$$

A symmetric matrix $\mathbf{A}$ can be decomposed into the product of two triangular matrix by the Cholesky decomposition [60] such as

$$\mathbf{A} = \mathbf{L}\mathbf{L}^{\mathrm{H}}, \tag{A.4}$$

where $\mathbf{L}$ is a lower triangular matrix.

A.1.3 Multivariate normal distribution definition

The $m \times 1$ random vector $\mathbf{X}$ is said to have an m-variate normal distribution if, for every $\alpha \in \mathrm{R}^{\mathrm{n}}$ the distribution of $\alpha'\mathbf{X}$ is univariate normal [50].

If $\mathbf{X}$ has an m-variate normal distribution then both $\mu = \mathrm{E}[\mathbf{X}]$ and $\mathbf{\Sigma} = Cov(\boldsymbol{X})$ exit and the distribution is determined by μ and $\mathbf{\Sigma}$, in other words $\mathbf{X} \sim \mathcal{N}(\mu, \mathbf{\Sigma})$.

A.2 Wishart matrix

Let us define the $m \times m$ random matrix $\mathbf{A} = \mathbf{H}\mathbf{H}^{\mathrm{H}}$, where the columns of the $m \times n$ matrix $\mathbf{H}$ are zero-mean independent real/complex Gaussian vectors with covariance matrix $\mathbf{\Sigma}$. Then, the matrix $\mathbf{A}$ is a Wishart Matrix with n degrees of freedom and covariance matrix $\mathbf{\Sigma}$, $\mathbf{A} \sim \mathrm{W}(n, \mathbf{\Sigma})$ for $n \geq m$ [61].

A.3 The chi-Square distribution

The Chi-Square distribution is obtained from a sum of squares of independent normal zero-one $\mathcal{N}(0, 1)$, random variables. We defined the Chi-Square distribution as in [60].

If $Y_1, Y_2, \cdots, Y_{\mathrm{n}}$ are independent normal random variables with mean $\mu_i = 0$ and variance $\sigma^2 = 1$, $Y_i \sim \mathcal{N}(0, 1)$, or, employing vector notation $\boldsymbol{Y} \sim \mathcal{N}(\mathbf{0}, \mathbf{1})$, then

$$Q = \boldsymbol{Y}'\boldsymbol{Y} = \sum_{i=1}^{n} \boldsymbol{Y}_i \sim \chi^2(n); \qquad 0 < Q < \infty, \tag{A.5}$$

$Q = \boldsymbol{Y}'\boldsymbol{Y}$ has a central χ^2 distribution with n degrees of freedom.

A.4 Wishart distribution

Let us define the Wishart distribution following [50, 62]. If $\mathbf{A} = \mathbf{Z}^{\mathrm{H}}\mathbf{Z}$, where the $m \times n$ matrix $\mathbf{Z}$ is $\mathcal{CN}(0, \mathbf{\Sigma})$, then $\mathbf{A}$ is said to have a Wishart distribution with n degrees of freedom and covariance matrix $\mathbf{\Sigma}$, $A \sim \mathrm{W}_m(n, \mathbf{\Sigma})$, the subscript of W denotes the size of $\mathbf{A}$.

Let $\mathbf{W}$ be Wishart distributed matrix with n degrees of freedom and unitary covariance

$$\mathbf{W} \sim W_m(n, \mathbf{I}), \quad \text{if } \ \boldsymbol{W} = \sum_{i=1}^{n} \boldsymbol{z}_i \boldsymbol{z}_i^{\mathrm{H}}\ , \ \boldsymbol{z}_i \text{ i.i.d. } \mathcal{CN}_p(\mathbf{0}, \mathbf{I}), \tag{A.6}$$

where, $\mathcal{N}_m(\mathbf{0}, \mathbf{I})$ is the m-multivariate normal distribution with zero vector mean and unitary covariance matrix. Suppose we have a covariance matrix $\mathbf{\Sigma} = \mathbf{A}\mathbf{A}^{\mathrm{H}}$, the $\boldsymbol{v} = \boldsymbol{A}\boldsymbol{z}$ and $\boldsymbol{V} = \sum_{i=1}^{n} \boldsymbol{v}_i \boldsymbol{v}_i^{\mathrm{H}}$, then using the result in A.3 the covariance of $\boldsymbol{v}$ is

$\mathbf{A}\mathrm{Cov}(\boldsymbol{z})\mathbf{A}^{\mathrm{H}} = \mathbf{A}\mathbf{A}^{\mathrm{H}} = \boldsymbol{\Sigma}$. Hence, $\boldsymbol{v}$ is $\mathcal{N}(0, \boldsymbol{\Sigma})$ and $\boldsymbol{V} \sim \mathrm{W}_m(n, \boldsymbol{\Sigma}))$. Furthermore,

$$\begin{aligned} \boldsymbol{V} &= \sum_{i=1}^{n} \boldsymbol{v}_i \boldsymbol{v}_i^{\mathrm{H}} \\ &= \sum_{i=1}^{n} (\mathbf{A}\boldsymbol{z}_i)(\mathbf{A}\boldsymbol{z}_i)^{\mathrm{H}} \\ &= \mathbf{A} \sum_{i=1}^{n} \boldsymbol{z}_i \boldsymbol{z}_i^{\mathrm{H}} \mathbf{A}^{\mathrm{H}} \\ &= \mathbf{A}\mathbf{W}\mathbf{A}^{\mathrm{H}}. \end{aligned} \tag{A.7}$$

If $m = 1$ and $\boldsymbol{\Sigma} = 1$, then this distribution is a Chi-Squared distribution with n degrees of freedom.

A.5 Bartlett's decomposition

Let $\boldsymbol{W}$ be $\mathrm{W}_m(n, \mathbf{I}_n)$, where $n \geq m$ is an integer, and put $\boldsymbol{W} = \boldsymbol{T}\boldsymbol{T}^{\mathrm{H}}$, where $\boldsymbol{T}$ is lower-triangular $m \times m$ matrix with positive diagonal elements. Then the elements $t_{(i,j)}$ $(1 \leq j \leq i \leq m)$ of T are all independent, $t_{i,i}^2$ is $\mathcal{X}_{n-i+1}^2$ $(i = 1, \ldots, m)$ and t_{ij} is $\mathcal{N}(0, 1)$ [50, 62].

We can extend this result for Wishart distributions with covariance matrix other than unitary using the result A.7 such that $\boldsymbol{V} = \mathbf{A}\mathbf{W}\mathbf{A}^{\mathrm{H}} = \mathbf{A}\boldsymbol{T}\boldsymbol{T}^{\mathrm{H}}\mathbf{A}^{\mathrm{H}}$, $\boldsymbol{V} \sim \mathrm{W}_m(n, \boldsymbol{\Sigma}))$, where $\boldsymbol{\Sigma} = \mathbf{A}\mathbf{A}^{\mathrm{H}}$ can be computed with the Cholesky decomposition A.4.

B Example of system level simulation output

The simulation results presented in this annex correspond to a 4x2 SU-MIMO system with ideal cell selection. The deployment scenario is 3GPP Case 1, with each eNB having 4 closely spaced cross-polarized antenna elements. The six studied linear receivers are simulated, and the output of the system simulation is presented.

The Figure A.1 depicts the achieved goodput CDF for the six simulated receivers. From the depicted CDF it can be observed that the 3 best performing receivers are the IRC, the LMMSE-IRC$_{\text{WI-RS}}$ and the LMMSE$_{\text{CL}}$ (also called option 2 receiver). Also, 70% of UEs utilizing theLMMSE-IRC$_{\text{WI-DATA}}$ perform worst than UEs utilizing the MRC receiver. Here goodput is defined as the successfully transmitted useful data, meaning that the control channel data and reference symbols are not taken into account in the throughput calculation.

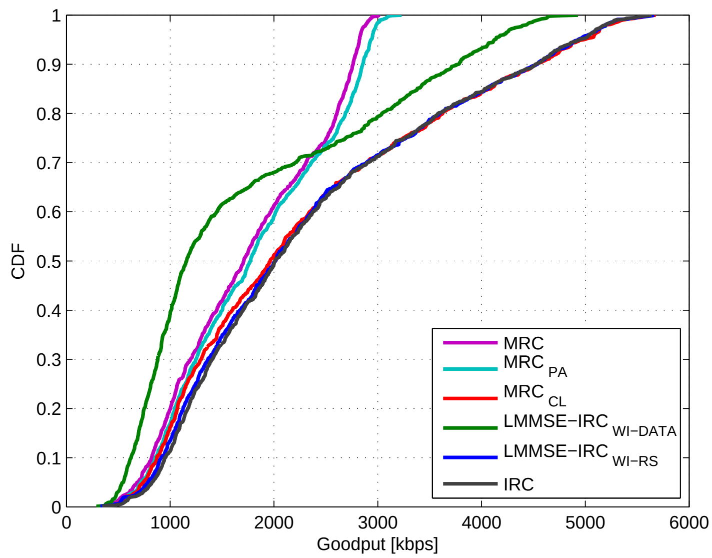

Figure A.1: Goodput, 3GPP Case 1, 4x2 XP $\lambda/2$, HO= 0 dB

The following Table A.1 shows a compact summary of performance taken from the CDFs of Figure A.1. The mean SE stands for mean spectrum efficiency and it is expressed in bps/Hz/Sector. The 5% SE stands for the 5% point of the CDF spectral efficiency (or cell-edge spectral efficiency), which is a effective measure to calculate the spectral efficiency experienced by cell-edge UEs. The 5% SE is expressed in bps/Hz/Sector/UE.

Table A.1: System Performance, 3GPP Case 1, 4x2 XP $\lambda/2$, HO= 0 dB

	mean SE $\left[\frac{bps/Hz}{Sector}\right]$	*Gain(%)*	5% SE $\left[\frac{bps/Hz}{Sector/UE}\right]$	*Gain(%)*
MRC	1.740	-	0.064	-
MRC_{PA}	1.807	*3.9*	0.067	*4.9*
LMMSE_{CL}	2.309	*32.7*	0.068	*7.1*
$\text{LMMSE-IRC}_{\text{WI-DATA}}$	1.766	*1.5*	0.051	*-19.3*
$\text{LMMSE-IRC}_{\text{WI-RS}}$	2.335	*34.2*	0.071	*11.3*
IRC	2.355	*35.4*	0.075	*18.1*

Every UE deployed in the simulation area has a different geometry factor, thus an effective manner to visualize the goodput each receiver achieves at different geometry positions is depicted in Figure A.2. From the goodput vs. geometry figure plus combining the information given by Figure A.1, it is observed that 70% of UEs have a geometry below 11 dB for this particular simulated case.

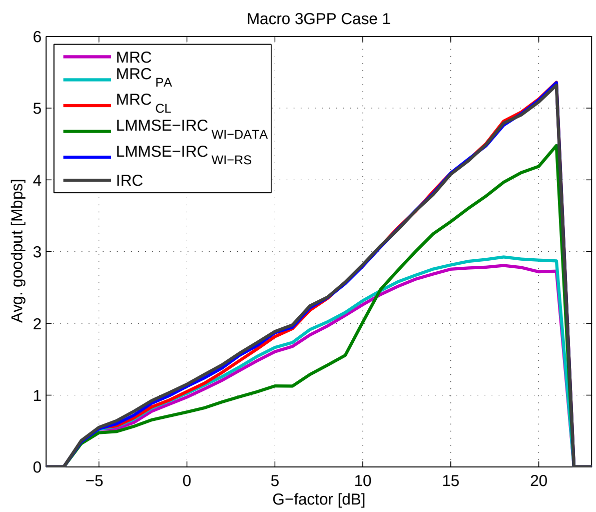

Figure A.2: Goodput vs. geometry, 3GPP Case 1, 4x2 XP $\lambda/2$, HO= 0 dB

The rank probability is defined as the used number of layers used for transmission divided by the total number of transmissions. The rank probability is depicted in Figure A.3. From the figure it can be observed that the receivers that reduce the co-layer interference make the system to utilize more dual layer transmission than receivers that do not reduce the co-layer interference.

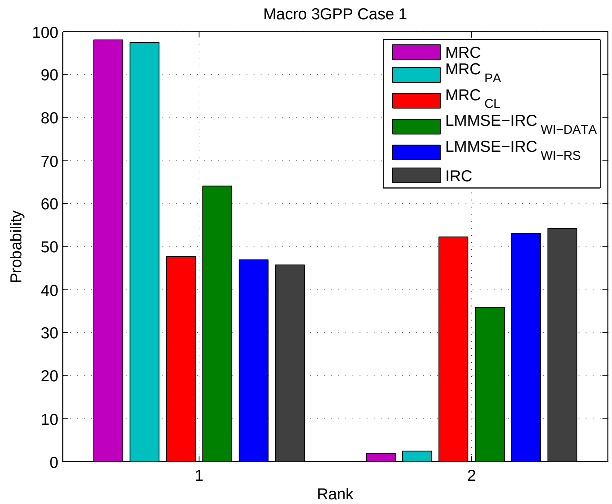

Figure A.3: Rank probability, 3GPP Case 1, 4x2 XP $\lambda/2$, HO= 0 dB

The block error probability (BLEP) is depicted in Figure A.4. The outer loop link adaption target has been set to 10% BLEP. This means that the probability that the first transmission succeeds should be 90%. From Figure A.4, it is observed that the data-sample-based advanced receiver does not achieve the 10% target which is not desirable.

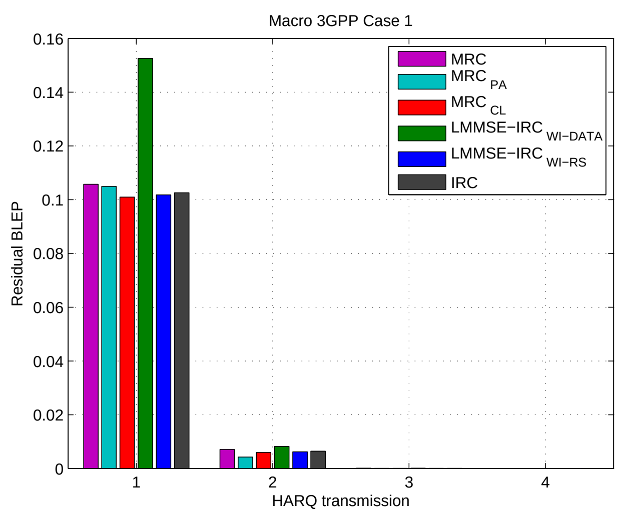

Figure A.4: HARQ, 3GPP Case 1, 4x2 XP $\lambda/2$, HO= 0 dB